

# Exploring the grand-canonical phase diagram of interacting bosons in optical lattices by trap squeezing

Tommaso Roscilde<sup>1</sup>

<sup>1</sup>*Laboratoire de Physique, École Normale Supérieure de Lyon, 46 Allée d'Italie, 69007 Lyon, France*

In this paper we theoretically discuss how quantum simulators based on *trapped* cold bosons in optical lattices can explore the grand-canonical phase diagram of *homogeneous* lattice boson models, via control of the trapping potential independently of all other experimental parameters (trap squeezing). Based on quantum Monte Carlo, we establish the general scaling relation linking the global chemical potential to the Hamiltonian parameters for the Bose-Hubbard model in a parabolic trap, describing cold bosons in optical lattices; we find that this scaling relation is well captured by a modified Thomas-Fermi scaling behavior - corrected for quantum fluctuations - in the case of high enough density and/or weak enough interactions, and by a mean-field Gutzwiller Ansatz over a much larger parameter range. The above scaling relation allows to control experimentally the chemical potential, independently of all other Hamiltonian parameters, via trap squeezing; given that the global chemical potential coincides with the local chemical potential in the trap center, measurements of the central density as a function of the chemical potential gives access to the information on the *bulk* compressibility of the Bose-Hubbard model. Supplemented with time-of-flight measurements of the coherence properties, the measurement of compressibility enables one to discern among the various possible phases realized by bosons in an optical lattice with or without external (periodic or random) potentials - *e.g.* superfluid, Mott insulator, band insulator, and Bose glass. We theoretically demonstrate the trap-squeezing investigation of the above phases in the case of bosons in a one-dimensional optical lattice, and in a one-dimensional incommensurate superlattice.

PACS numbers: 03.75.Lm, 71.23.Ft, 68.65.Cd, 72.15.Rn

## I. INTRODUCTION

The impressive recent advances in the engineering of interacting Hamiltonians for cold trapped atoms suggest the possibility of experimentally determining the equilibrium (and out-of-equilibrium) behavior of fundamental theoretical quantum many-body models. In particular experiments on cold atoms in optical lattices have demonstrated the ability of implementing fundamental lattice models (of Hubbard type) with full tunability of all Hamiltonian parameters, as well as of the lattice geometry and dimensionality [1, 2]. Remarkably, the understanding of a large class of lattice many-body models (such as interacting fermions, frustrated quantum magnets, etc.) keeps defying standard theoretical and computational approaches. Hence, the perspective of realizing analog quantum simulators [3] based on cold atoms, literally implementing the physics of the challenging models in question, represents a most promising and innovative route towards their understanding.

Nonetheless, several obstacles still separate the current experiments from giving original answers to long-standing questions in quantum many-body physics on a lattice. One problematic feature of cold-atom systems in a lattice is thermometry [9–13, 16? ]: given that trapped cold atoms are not coupled to a thermal reservoir, their entropy can be controlled but not their temperature, and the knowledge of the temperature as a function of entropy is a problem which requires the prior knowledge of the equation of state of the many-body system under investigation [12, 17, 18]. A second puzzling feature of

current cold-atom experiments - which will be the main concern of this paper - is the intrinsic *inhomogeneity* of these systems, imposed by the presence of an overall parabolic trapping potential. While the size of the lattices realized in experiments can easily beat the capability of current classical simulation methods (at least in dimensions  $d > 1$ ), the parabolic potential significantly limits the size of the lattice over which a uniform phase of the Hamiltonian model is realized. Indeed, a parabolic trapping potential  $V(i) = V_t(r_i - r_0)^2$  (where  $r_i$  is the position of the  $i$ -th lattice site and  $r_0$  is the center of the trap) imposes a site dependent chemical potential and site-dependent energy jumps  $\Delta E(i) = V(i+1) - V(i) = V_t(r_{i+1} - r_i)(r_{i+1} + r_i - 2r_0)$  between nearest-neighboring sites. If the local many-body phase at a given filling  $n$ , realized around  $i$ -th site at the local chemical potential  $\mu(i) = V(i)$ , is not protected by a particle/hole gap  $\Delta_g \gg \Delta E(i)$ , its existence is necessarily restricted to a narrow neighborhood of site  $i$ . This aspect introduces significant limitations in the capability of realizing phases which are particularly sensitive to the filling, and which display a small or no particle/hole gap over the ground state (see *e.g.* the supersolid phase of strongly correlated bosons [5–7] or the Bose-glass [8] for bosons in a random potential).

In principle one could consider the coexistence of several different phases in the trap as an advantage, given that one single experiment samples a significant portion of the phase diagram of the Hamiltonian implemented in the system via the chemical potential modulation imposed by the trap. [19, 20] Unfortunately this form of

“parallelism” is generally hard to enjoy, as most measurement protocols for trapped cold atoms employed to date give access to *global* observables, which collect a signal from all the different regions of the trap. This fact becomes particularly inconvenient when considering the measurement of the excitation spectrum, as sampled *e.g.* via lattice-modulation and two-photon Bragg spectroscopy [21–24]. In fact it is quite difficult to associate the different contributions to the excitation spectrum with different spatial regions of the trap, a fact which makes it very hard to extract precise information on the structure of the excitations associated with a particular phase of interest. In particular, the presence of a trap imposes the existence of a halo of dilute particles at the cloud boundary, which in principle can always host low-energy excitations. Consequently, the fundamental question of the presence or absence of an energy gap over the ground state of a particular phase, realized locally in the trap, becomes a formidable task for current cold-atom simulators.

It is important to mention that single-site addressability in optical lattices is becoming reality in recent experiments on quantum gas microscopy [25–29]. This achievement definitely allows one to enjoy the above mentioned parallelism in the chemical potential exhibited by trapped experiments [19], but only at the level of *local* properties, defined on spatial regions over which the variation of the local chemical potential can be considered weak; and only as long as the so-called local-density approximation can be fully trusted. Yet *non-local* properties of homogeneous phases, including correlation functions and collective excitations, cannot be extracted from an inhomogeneous sample, except for those associated with the region of maximal homogeneity, namely the trap center.

In this paper we propose an experimental protocol which aims at circumventing most of the difficulties listed above, while taking advantage of the trap as a low-energy probe for the properties of the system (trap-squeezing spectroscopy [30]). The fundamental idea relies on the fact that trap effects are minimal in the center, both  $V(i)$  and  $\Delta E(i)$  vanish, so that a local, homogeneous phase can be established over a significant portion of the system, roughly of the order of  $\sim 10$  lattice sites in each spatial direction. This sizable portion of the lattice can be now regarded as the *system* of interest, while the rest of the lattice as the *environment*, acting in particular as a particle reservoir (see Fig. 1 for a sketch). In light of the above discussion, we can conclude that the trap center realizes the “textbook” quantum simulation of the particular Hamiltonian implemented in the system in the grand canonical ensemble (namely at a nearly *uniform* local chemical potential). What remains to be shown is how to control the crucial parameter of the quantum simulation at the trap center, namely its local chemical potential, and how to retrieve selective information on the local collective phase realized there.

We here specialize our discussion to the case of bosons

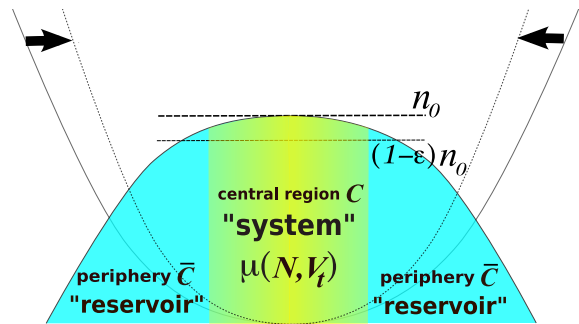


FIG. 1: An atomic cloud in a smoothly varying trapping potential - such as a parabolic trap - can be virtually divided into two regions: a central  $C$  region over which the density is essentially uniform (within a tolerance  $\epsilon$ ), and whose local chemical potential  $\mu(N, V_t)$  essentially corresponds to the global chemical potential of the atomic cloud; and a periphery region  $\bar{C}$ , in which the density varies rapidly in space, due to the trapping potential. The nearly homogeneous central region can be regarded as the “system” in a grand-canonical ensemble, while the periphery can be regarded as a particle “reservoir”. Increasing the trapping potential (as indicated by the black arrows) increases the chemical potential of the reservoir  $\bar{C}$ , and, at equilibrium, that of the system  $C$ . Hence the chemical potential of the system can be controlled continuously by the trapping potential  $V_t$ .

in optical lattices, governed by the Bose-Hubbard Hamiltonian in an external potential, and leaving the case of fermions to future work. In particular we quantitatively discuss how, tuning the trap frequency independently of all others experimental parameters, one gains direct access to the control of the chemical potential in the trap center. Remarkably, numerical simulations on the Bose-Hubbard model on the hypercubic lattice show that there exists a simple relation between the strength of the trapping potential and the chemical potential: this relation follows approximately the predictions which can be obtained both from the atomic limit in a lattice, and from the Thomas-Fermi theory for weakly interacting gases in continuum space, with deviations due to quantum and lattice corrections. Remarkably, such deviations are quantitatively captured at the *mean-field* level. This means that, unlike the case of the temperature [17, 18], the accurate knowledge of the chemical potential of a strongly correlated bosonic system in an optical lattice might not require in general an extensive ab-initio calculation. This makes the trapping potential a fundamental experimental knob for the quantum simulation, whose effect on the system’s parameters can be readily assessed.

Nonetheless, the tuning of such a knob has to be done very carefully, and in general it cannot be done after loading the atoms in the optical lattices. In fact, increasing the strength of the trapping potential at equilibrium leads to the transfer of particles from the wings to the center of the trap, but the tunneling amplitude associated with such a transfer can be extremely small in strongly in-

interacting systems, requiring then exceedingly slow ramps of the trapping potential to enforce adiabaticity in the protocol. A simple way to circumvent this problem is proposed, based on the loading of atoms in the trap in the weakly interacting regime (namely without optical lattice) followed by the ramp of the optical lattice.

Once full control on the chemical potential at the trap center has been achieved, selective information can be retrieved on this region of space by microscopy of the atomic cloud. We here propose a measurement scheme of the average central density based on two tightly focused crossed beams resonant with different optical transitions of the atoms; as already mentioned, other quantum gas microscopy schemes (with resolution as high as one lattice spacing) have been proposed or even become experimentally available in the recent past. The knowledge of the central density as a function of the chemical potential provides then the fundamental information on the *bulk compressibility* of the Hamiltonian model implemented in the system, and hence on the particle/hole gap over the ground state. We present the application of trap-squeezing spectroscopy to the measurement of the bulk phase diagram of the Bose-Hubbard model in  $d = 1$ : in particular we discuss the case without any applied external potential, and the case in which an incommensurate potential with *two* wavelength components is applied to the system, giving rise to an extended Bose-glass phase whose compressible nature is perfectly captured via trap-squeezing spectroscopy.

The structure of the paper is then as follows. Section II introduces the model investigated, the local-density approximation and the fundamental role played by the average central density in the trap; Section III discusses the relationship between the chemical potential in the trap center and the trap strength for the Bose-Hubbard model in dimension  $d = 1, 2$ , and  $3$ , with or without an external potential; Section IV discusses the issue of equilibrium preparation of the system at a given trap strength, based on a two-step protocol for the ramp of the optical potentials; Section V discusses a proposal for the selective measurement of the average density in the trap center; applications to the Bose-Hubbard model without and with external superlattice potentials are presented in Section VI and VII respectively; Section VIII compares the central compressibility with the global compressibility of the atomic cloud, recently measured in experiments [31]; and finally Section IX is devoted to conclusions.

## II. LOCAL DENSITY APPROXIMATION, AVERAGE CENTRAL DENSITY AND CENTRAL CHEMICAL POTENTIAL

In this section we focus our attention to the general case of the Bose-Hubbard model on the  $d$ -dimensional hypercubic lattice in an external potential, composed of a rapidly varying part, given by a superlattice potential created by an additional standing wave applied to the

system [22, 32, 33], and a slowly varying parabolic part, coming from the overall gaussian profile of the lasers applied to the system.

$$\mathcal{H}(J, U, V_2, V_t) = \mathcal{H}_0(J, U, V_2) + V_t \sum_i (r_i - r_0)^2 n_i \quad (1)$$

$$\begin{aligned} \mathcal{H}_0(J, U, V_2) = & - J \sum_{\langle ij \rangle} (b_i^\dagger b_j + \text{h.c.}) + \frac{U}{2} \sum_i n_i (n_i - 1) \\ & + V_2 \sum_i g_i(\{\alpha_l\}, \{\phi_l\}) n_i \end{aligned} \quad (2)$$

where

$$g_i(\{\alpha_l\}, \{\phi_l\}) = \sum_{l=1}^d \cos^2(2\pi\alpha_l i_l + \phi_l) - \frac{d}{2} \quad (3)$$

is a one-color superlattice potential. Here  $i_l$  ( $l = 1, \dots, d$ ) are the coordinates of the  $i$ -th site and  $\langle ij \rangle$  are the pairs of nearest neighbors on the  $d$ -dimensional hypercubic lattice of size  $L^d$ .

Experiments on cold atoms in optical lattices are typically performed with a *fixed* number of particles  $N$ . Nonetheless, given that the particle number is a good quantum number of the Hamiltonian, at  $T = 0$  the system will be in a definite  $N$ -sector even in the grand-canonical ensemble. This allows us to regard the canonical system with  $N$  particles as equivalent to a system in the grand-canonical ensemble with Hamiltonian

$$\mathcal{H}_\mu = \mathcal{H} - \mu \sum_i n_i \quad (4)$$

where  $\mu = \mu(V_t, N, J, U, V_2)$  is the chemical potential which establishes  $N$  particles in the ground state of the Hamiltonian  $\mathcal{H}(J, U, V_2, V_t)$ . Moreover we can rewrite Eq. (4) as

$$\mathcal{H}_\mu = \mathcal{H}_0 - \sum_i \mu(i) n_i \quad (5)$$

where we have introduced the site-dependent chemical potential  $\mu(i) = \mu - V_t(r_i - r_0)^2$ . If  $\mu(i)$  is a slow-varying function in space around the reference site  $i^*$  over the typical length scale given by the correlation length of the Hamiltonian  $\mathcal{H}_{\mu(i^*)} = \mathcal{H}_0 - \mu(i^*) \sum_i n_i$ , one can adopt the local-density approximation (LDA): this amounts to considering that the trapped system behaves around the site  $i^*$  in the same way as its bulk counterpart at the homogeneous chemical potential  $\mu = \mu(i^*)$ . In particular, in absence of a superlattice potential, the local density  $\langle n_i \rangle$  for  $i \approx i^*$  will be extremely close to the homogeneous density in the ground state of  $\mathcal{H}_{\mu(i^*)}$ . In presence of a superlattice potential, the local density  $\langle n_i \rangle$  will be very close to the density of the bulk system at a point experiencing the same superlattice potential; moreover the average density over a period of the superlattice (or quasi-period

for incommensurate superlattices) centered around the site  $i^*$  will approximate very well the average density in the ground state of the bulk system. All these expectations for the behavior of the density are fully verified by numerically exact calculations on the Bose-Hubbard model with or without a superlattice [34–36]. The LDA typically breaks down when the local chemical potential  $\mu(i)$  approaches a critical value sitting at the boundary between two phases in the bulk system, so that the correlation length of the bulk system diverges.

The validity of the local-density approximation for parabolic traps implies that the trapped system faithfully probes the density of the bulk system at many different values of the chemical potential away from critical points. As mentioned in the introduction, this form of “parallel” sampling of the bulk phase diagram is only valid for local properties, and it cannot be exploited experimentally unless single-site addressability is achieved. On the contrary, imaging of the atomic cloud over a length scale  $R$  of  $5 - 10\mu\text{m}$  (corresponding to  $\sim 10 - 20$  lattice sites of an optical lattice with  $\lambda \sim 800$  nm) can be achieved more conventionally via large-aperture optics [37] (see Section V for a more detailed discussion). This means that the information on the local density can be retrieved if  $\langle n_i \rangle$  does not change appreciably over the lengthscale  $R$ . For a weak enough trapping potential, such a condition can be easily met at the *trap center*, where the variation in the local chemical potential is the slowest. We hence introduce the *average central density*

$$n_C =: \frac{1}{|C|} \sum_{i \in C} \langle n_i \rangle \quad (6)$$

where  $|C|$  is the size of the  $C$  region built around the trap center  $i_0$ . The  $C$  region is then defined as verifying a condition of quasi-homogeneity

$$\frac{|n_C - \langle n_{i_0} \rangle|}{\langle n_{i_0} \rangle} \leq \epsilon \quad (7)$$

with  $\epsilon \ll 1$ . Another important observation singles out the trap center as the most interesting region of the trap. Indeed, even when it is possible to measure the density at the single-site level, one can exclusively achieve the knowledge of a local observable  $A_i$  which, via the LDA, can be associated with that ( $A$ ) of the bulk system as a function of the chemical potential,  $A(\mu) \simeq A_i(\mu_i = \mu)$ . The complementary information on the non-local correlation functions of the bulk system is instead completely missing, and indeed the trapped system cannot faithfully reproduce the correlation properties of the bulk system in general (as testified by the poor performance of the LDA at the level of correlations [36]). Nonetheless, the trapped system can faithfully reproduce the correlations around the trap center over a length scale corresponding to the extent of the quasi-homogeneous central region. This aspect will be discussed in details in Section VI, where it will be shown in addition that the evolution of global correlation properties of the system (as probed

*e.g.* by time-of-flight measurements) is dominated by the evolution of correlations in the trap center, so that correlations in the trap center can effectively be accessed in the experiments.

The quasi-homogeneity condition Eq. (7) allows to identify  $n_C$  as a close approximation to the ground-state density of the bulk Hamiltonian Eq. (4) (with  $V_t = 0$ ) at a chemical potential corresponding to the background chemical potential  $\mu(V_t, N, J, U, V_2)$  of the trapped system. As further elaborated in Section V,  $n_C$  is experimentally accessible with conventional methods. In order to convert the information on  $n_C$  into information on the bulk phase diagram of the Hamiltonian  $\mathcal{H}_0$  of Eq. (2), we need to know at which chemical potential the experiment is operating once the experimental parameters  $V_t, N, J, U$  and  $V_2$  are set. This is the goal of next Section.

### III. TRAP-SQUEEZING CONTROL OF THE CHEMICAL POTENTIAL

In this section we investigate the dependence of the background chemical potential  $\mu(V_t, N, J, U, V_2)$ , stabilizing a ground state with  $N$  particles, for the Bose-Hubbard Hamiltonian with parameters  $J, U$  in a trapping potential of strength  $V_t$  and, generally, in a superlattice potential of strength  $V_2$ . We review the conventional Thomas-Fermi approximation and its generic prediction for the functional form of  $\mu$  in the general case of a  $d$ -dimensional hypercubic lattice. Remarkably, a numerical investigation based on numerically exact quantum Monte Carlo shows that the Thomas-Fermi prediction, modified by quantum fluctuations, is rather accurate at least in the regime of either weak enough interaction or high enough density. As a result, the chemical potential turns out to be simply controlled in the experiments either via the control on the particle population  $N$  or the trap strength  $V_t$ , or on both.

#### A. Atomic limit and Thomas-Fermi approximation

A simple theoretical approach giving the relationship between the chemical potential and the other Hamiltonian parameters for the Bose-Hubbard model is the atomic limit (AL), which consists in discarding the quantum kinetic term in the Hamiltonian and in solving for the diagonal part. Such an approximation is reasonable in the strongly interacting and strongly trapped limit  $U, V_t R^2 \gg J$ , where  $R$  is the radius of the atomic cloud. Minimizing the potential energy part with respect to the density

$$\mathcal{H}_{\text{pot}} = \frac{U}{2} \sum_i n_i(n_i-1) + V_2 \sum_i g_i n_i + V_t \sum_i i^2 n_i - \mu \sum_i n_i \quad (8)$$

one finds

$$n_i = \frac{\mu + U/2 - V_2 g_i - V_t (r_i - r_0)^2}{U}. \quad (9)$$

Imposing the condition  $N = \sum_i n_i$  and passing from the lattice to the continuum formulation, one readily obtains the AL chemical potential for a  $d$ -dimensional system

$$\begin{aligned} \mu_{\text{AL}} + \frac{U}{2} &= \left( \frac{d+2}{2} \frac{\Gamma(d/2+1)}{\pi^{d/2}} \right)^{\frac{2}{2+d}} (U N)^{\frac{2}{2+d}} V_t^{\frac{d}{2+d}} \\ &= \begin{cases} 0.82548\dots (U N)^{2/3} V_t^{1/3} & (d=1) \\ 0.79788\dots (U N V_t)^{1/2} & (d=2) \\ 0.81346\dots (U N)^{2/5} V_t^{3/5} & (d=3) \end{cases} \end{aligned} \quad (10)$$

Notice that the superlattice term does not enter in this formula because it has been chosen so as to take symmetric values around zero, and therefore it vanishes upon spatial integration.

On the other hand, a similar formula to Eq. (13) can be obtained in the weakly interacting case via a standard Gross-Pitaevskii (GP) approach plus a Thomas-Fermi (TF) approximation [38]. Taking the mean-field approximation  $a_i \approx \Psi_i$ ,  $a_i^\dagger \approx \Psi_i^*$  on the normal ordered Hamiltonian Eq. (1) (where  $\Psi_i$  is the condensate wavefunction) one obtains the lattice GP energy functional

$$E_{\text{GP}} = -J \sum_{\langle ij \rangle} (\Psi_i^* \Psi_j + \text{c.c.}) + \frac{U}{2} \sum_i |\Psi_i|^4 + \sum_i (V_i - \mu) |\Psi_i|^2 \quad (11)$$

where  $V_i = V_2 g_i + V_t (r_i - r_0)^2 - \mu$ .

The standard TF approximation consists in neglecting completely the kinetic term in the Gross-Pitaevskii functional. This is justified in the continuum case because the kinetic energy is suppressed when the wavefunction is slowly varying in space; on the other hand, in the lattice case, a slowly varying wavefunction is such that  $\Psi_i^* \Psi_j \approx |\Psi_i|^2$ , namely the kinetic term does not cancel, but it effectively adds up to the chemical potential term,  $\mu \rightarrow \mu - 2dJ$ . Minimizing the GP functional leads then to the lattice TF equation for the density:

$$|\Psi_i|^2 = \frac{\mu + 2dJ - V_2 g_i - V_t (r_i - r_0)^2}{U} \quad (12)$$

Integrating over space in the continuum limit leads to the result  $\mu_{\text{TF}} = -2dJ + \mu_{\text{AL}} + U/2$ .

The central prediction is the linear dependence of  $\mu$  on the combination  $(N^2 V_t^d)^{1/(2+d)}$ , with a slope dependent on  $U^{2/(2+d)}$ : both predictions will be verified by a numerically exact calculation in a large parameter regime. What is completely missing in the above simple approach are: 1) lattice commensuration effects, relevant in the case of the appearance of band/Mott insulator states (given that the analytical expression Eq. (10) is obtained in the continuum limit); 2) a proper treatment of the quantum kinetic  $J$ -term in the Hamiltonian. The lattice effects can be readily restored by numerically performing

the sum  $N = \sum_i n_i$  instead of analytically integrating the continuum generalization of Eq. 9, at the expense of losing the closed-form prediction of Eq. (10). On the other hand, a full account of the quantum corrections requires a more extensive numerical treatment. This will be provided in the following, where we will see that such effects do not alter too drastically the TF/AL predictions, and they can be captured already at the mean-field level.

## B. Quantum Monte Carlo results

Here we present the results of quantum Monte Carlo simulations of the  $d$ -dimensional Bose-Hubbard model on  $L^d$  hypercubic lattices, based on the Stochastic Series Expansion method with directed-loop updates [39]. We have performed simulations at low temperatures  $T \sim J/L$  in order to remove significant thermal effects. We perform the simulation in the grand-canonical ensemble, and we fine-tune the chemical potential  $\mu$  which stabilizes a given particle number  $N$  for the Hamiltonian Eq. (1); this allows us to numerically sample the function  $\mu(V_t, N, J, U, V_2)$ . In the following we take  $J$  as the energy scale, and express all other quantities in units of  $J$ . We have performed the simulations for two values of the  $U/J$  ratio for each dimensionality  $d$  and both for zero superlattice potential ( $V_2 = 0$ ) and for an intense superlattice potential ( $V_2 = U$ ). We have considered both incommensurate superlattices ( $\alpha = 830/1076$  as in the experiment of Ref. 22) and commensurate ones ( $\alpha = 3/4$  and  $1/2$ ). Results for one spatial dimension have already been partially reported in Ref. 30.

### 1. $d=1$ without superlattice

We begin our discussion with the case of absence of a superlattice ( $V_2 = 0$ ). Figs. 2 and Figs. 3 show results for the two complementary regimes of  $U/J = 5$  and  $U/J = 20$ . Judging from the phase diagram of the 1d Bose-Hubbard model [40], for  $U/J = 5$  the kinetic and the potential part of the bulk Hubbard Hamiltonian are in strong competition for most filling values  $n \lesssim 3$ , so that a variation of the chemical potential brings the system through an alternation of correlated superfluid phases and Mott insulating phases separated by quantum critical points. Despite the important quantum effects taking place in the system, it is remarkable to observe in Fig. 2 that all  $\mu$  values obtained by various combinations of  $V_t$  and  $N$  collapse onto the same universal curve, which is a homogeneous function of  $N^2 V_t / J$ , in agreement with the AL/TF prediction Eq. (10). Refs. [41, 42] have introduced the so-called ‘‘characteristic density’’,  $\tilde{\rho} = N(V_t/J)^{d/2}$ , as the relevant parameter to characterize the density of a trapped system in  $d$ -dimensions. Our data suggests that the chemical potential is a homogeneous function of the characteristic density. This result will be further confirmed in the case  $d = 2, 3$ ; see

also Sec. III D for a general discussion.

Even more remarkably, for large enough  $N$  and/or  $V_t/J$  values, the universal curve obeys a modified TF (mTF) scaling of the kind

$$\mu_{\text{mTF}}(V_t, N, J, U, V_2)/J = C_d (U/J)^{\frac{2}{2+d}} + \gamma_d (U/J N)^{\frac{2}{2+d}} (V_t/J)^{\frac{d}{2+d}} \quad (13)$$

where  $C_d = C_d(U/J, V_2/J)$ . Here  $\gamma_d$  is a  $d$ -dependent slope: numerical evidence shows that  $\gamma_d$  does *not* seem to depend on the other Hamiltonian parameters (see Ref. 30, and the discussion below). A fit to the  $d = 1$  data for  $U/J = 5$  gives us  $\gamma_{d=1} = 0.817(2)$ , which compares surprisingly well with the AL/TF prediction of Eq. (10). Moreover  $C_d$  is a  $d$ -dependent offset term which is also found to depend on  $U/J$  and on  $V_2/J$ , and which contains the most relevant quantum corrections to the TF/AL result. It is important to stress that in general  $C_d (U/J)^{\frac{2}{2+d}}$  is *not* the correct value of  $\mu/J$  for  $V_t/J, N \rightarrow 0$ . In fact in this limit the system becomes extremely dilute and the dependence on  $U/J$  should drop out. Indeed, in the limit of low  $N$  and  $V_t$ , the  $\mu$  curve crosses over to the correct dilute limit (see inset of Fig. 2) which gives the well known result  $\mu(N = 0, V_t = 0) = -2dJ$  as obtained from the solution of the tight-binding model. As seen in Sec. III A this result coincides with the  $N = 0, V_t = 0$  value predicted by the lattice TF theory (Eqs. (10) and (12)) – as it should be expected, given that, in the dilute limit, the bose gas becomes ideal. This also means that the quantum offset term ( $-2dJ$ ) of the chemical potential from lattice TF theory does not correspond at all to the quantum correction appearing in the mTF scaling, Eq. (13). Hence the form of Eq. (13) is far from being trivial.

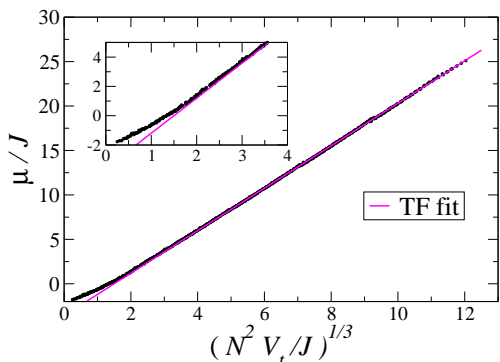


FIG. 2: Chemical potential for the 1d Bose-Hubbard model with  $U = 5J$ . The universal curve  $\mu = \mu(N^2 V_t/J)$  has been obtained via the collapse of many data sets, with  $N = 20, \dots, 120$  and  $V_t = 0.004, \dots, 0.140J$ . The solid curve is a linear fit to the Ansatz Eq. (13). Inset: zoom on the crossover from the mTF behavior to the low- $N$  and low- $V_t$  behavior.

The results for  $U = 20J$  are instead more elaborate. In this case the inspection of the 1d Bose-Hubbard phase diagram reveals that the system with a filling  $n \lesssim 3$  is

a Mott insulator for most of the chemical potential values. Hence the lattice stabilizes commensurate insulating regions in the trap which are completely missed in the continuum limit leading to the AL/TF formula Eq. (10). Nonetheless it is remarkable to observe that all the data obtained for different  $N$  and  $V_t$  values collapse onto the same universal curve which is again a homogeneous function of  $N^2 V_t$ , consistently with the AL/TF prediction. Yet this curve shows a succession of kinks separating various regimes of filling and trapping: an inspection in the microscopic structure of the states corresponding to the various regions shows that each kink marks the appearance of particles in a new “shell” of the trapped cake structure of the density profile (see Fig. 3(a)). When the system has filling  $\langle n_i \rangle < 1$  throughout the trap, the large  $U/J$  value suppresses multiple occupation and the system behaves effectively as a hardcore-boson system. This is shown by the excellent agreement between the low- $N$ /low- $V_t$  data for the softcore boson system and the same data for a hardcore-boson system which can be obtained exactly by standard Jordan-Wigner diagonalization [43]. Increasing the filling and/or the trapping, the condition of single occupancy is eventually violated and the second shell of the cake starts to be filled. In the AL, the condition for the presence of a site with occupation  $n = 2$  in the center of the trap in a 1d system is  $V_t (N/2)^2 \geq U$  which gives the critical value  $(N^2 V_t/J)_{n=2} = 4 U/J$ . Assuming that the population of further shells appears upon depletion of the shell with single occupancy, we find that the  $n = 3$  shell starts being occupied when

$$V_t (N_1/2)^2 = V_t (N_2/2)^2 + U = 2U \quad (14)$$

which means that the  $n = 2$  shell stops growing upon increasing  $V_t$  and the  $n = 3$  shell starts building up. Here  $N_i$  indicates the number of particles in the  $i$ -th shell. With the condition  $N_1 + N_2 = N$  Eq. (14) gives

$$(N^2 V_t/J)_{n=3} = 4(1 + \sqrt{2})^2 U/J \quad (15)$$

A similar reasoning leads to the critical value for the population of the  $n = 4$  shell

$$(N^2 V_t/J)_{n=4} = 2(1 + \sqrt{2})^2(1 + \sqrt{3})^2 U/J \quad (16)$$

and so on. Hence for  $U = 20J$  we obtain  $(N^2 V_t/J)_n = 80, 466.27, \text{ and } 1740.16$  for  $n = 2, 3, \text{ and } 4$ ; the corresponding numerical estimates from the QMC simulations are  $(N^2 V_t/J)_n \approx 66, 400 \text{ and } 1200$  which, not surprisingly, is lower than the AL prediction due to quantum effects allowing the particles to tunnel from the wings of the cloud into the center at a lower trapping strength/particle number.

It is evident from Fig. 3 that lattice commensuration effects become weaker and weaker on the  $\mu$  curve for increasing filling. In particular, when plotting the curve as a function of the natural TF parameter  $(N^2 V_t/J)^{1/3}$ , as done in Fig. 3(c), we observe that the mTF scaling of

Eq. 13 sets in approximately once the  $n = 3$  shell starts to be filled. A fit of the large- $N$ /large- $V_t$  data with Eq. 13 delivers a value of  $\gamma_{d=1}$  consistent with the value obtained from the  $U/J = 5$  data, confirming that  $\gamma_d$  only depends on dimensionality.

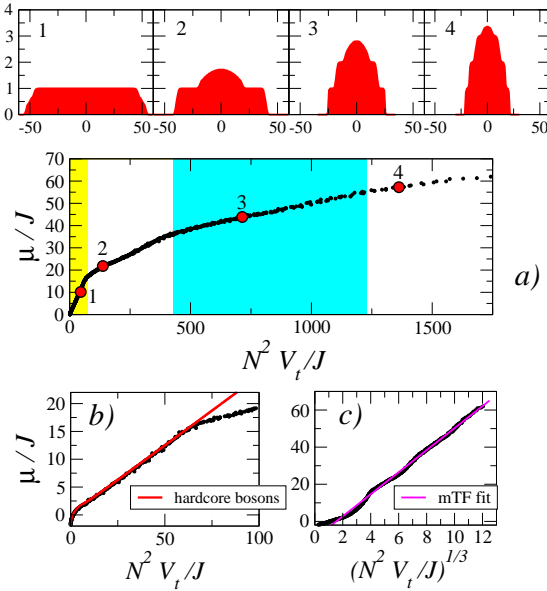


FIG. 3: Chemical potential for the 1d Bose-Hubbard model with  $U = 20 J$ . *a)* Main panel: Universal curve  $\mu = \mu(N^2 V_t/J)$ . The curve is obtained via the collapse of many data sets (same parameters as in Fig. 2). The differently colored regions correspond to the number of shells populated in the “wedding cake” structure, from 1 up to 4. Upper panels: four representative density profiles showing four different shell occupations ( $N = 100$  and  $V_t = 0.004, 0.014, 0.070$  and  $0.135 J$ ). *b)* Zoom on the low- $N$ /low- $V_t$  region (first shell occupied only), showing agreement with the corresponding data for a hardcore boson system. *c)* Universal curve presented as a function of  $N^{2/3}(V_t/J)^{1/3}$ : the solid curve represents a linear fit to the Ansatz Eq. (13).

## 2. $d=1$ with superlattice

Fig. 4 shows the  $\mu$  curve for the 1d Bose-Hubbard model in a strong superlattice with  $\alpha = 3/4$ ,  $\phi = 0$  and  $V_2 = U$ , and for three values of  $U/J = 10, 20$  and  $30$ . Again the chemical potential is clearly a homogeneous function of  $N^2 V_t/J$ , as shown by the collapse of all the  $\mu$  values onto the same universal curve dependent on  $U/J$  and  $V_2/J$ . For large  $U/J$ ,  $V_2/J$  and/or for small  $N^2 V_t/J$  we observe kinks in the  $\mu$  curve characteristic of lattice commensuration effects: in the case of a commensurate superlattice as the one considered here these effects are clearly related to the fractional filling shells [30] appearing in the AL of the system at fillings  $(2n + 1)/4$  with  $n = 0, 1, 2, \dots$ . Yet the overall trend of the curve for high

enough filling follows the mTF behavior Eq. 13, and a fit to that equation gives again a  $\gamma_d$  consistent with what found in the previous section in absence of the superlattice. This confirms the TF/AL prediction that the presence of a superlattice is not influencing the overall slope of the  $\mu$  curve. Similar curves for the incommensurate superlattice case  $\alpha = 1076/830$  have already appeared in Ref. 30.

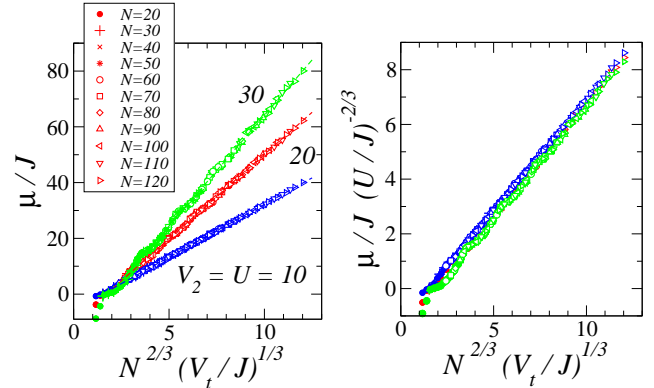


FIG. 4: Chemical potential for the trapped 1d Bose-Hubbard model with a commensurate superlattice potential ( $V_2 = U, \alpha = 3/4$ ). The right panel shows that all curves have a universal scaling of the slope with the ratio  $U/J$ . Dashed lines are fits to the Ansatz Eq. (13).

It is important to stress that lattice commensuration effects in the presence of a superlattice are strongly related to the possibility of maintaining the spatial phase  $\phi$  of the superlattice fixed in the experiments. If this phase is allowed to fluctuate, (as it generally happens from shot to shot of the same experiment [44], unless phase locking is explicitly enforced [32]), the chemical potential in the experiment is going to change accordingly, assuming that all other experimental parameters remain unchanged. In this case it is then more convenient to introduce a *phase-averaged* chemical potential  $\langle \mu \rangle_\phi$  - namely averaged over random fluctuations of the phase  $\phi$ . Fig. 5 shows  $\langle \mu \rangle_\phi$  for two superlattices: for the commensurate one discussed above, and for an incommensurate one which has one additional color component, namely

$$g_i(\alpha, \alpha', \phi, \phi') = \cos^2(2\pi\alpha i + \phi) + \cos^2(2\pi\alpha' i + \phi') - 1 \quad (17)$$

with  $\alpha = 1076/830$  and  $\alpha' = 1473/830$ . This particular superlattice will be further discussed in Section VII. The chemical potential values are typically averaged over a sample of  $\sim 100 - 200$  phase values. Comparing the average results with typical ones we notice that fluctuations are small around the average, so that, for each different

$U/J$	$V_2$	$\alpha$	$\gamma_{d=1}$	$C_{d=1}$
5	0	-	0.818(1)	-1.23(1)
10		-	0.818(2)	-1.21(2)
20		-	0.815(5)	-1.32(4)
10	$U$	$3/4$	0.817(2)	-1.23(2)
20		$3/4$	0.820(2)	-1.40(1)
30		$3/4$	0.822(3)	-1.58(1)
10	$U$	$830/1076$	0.816(3)	-1.22(3)
20		$830/1076$	0.822(4)	-1.42(4)
30		$830/1076$	0.819(5)	-1.54(5)

TABLE I: Results of the fit of the chemical potential data to the scaling Ansatz, Eq. (13), for the 1d trapped Bose-Hubbard model without any superlattice, and with a commensurate/incommensurate superlattice.

realization of the superlattice, the average chemical potential  $\langle \mu \rangle_\phi$  stabilizes in the system a number of particles  $N$  which is close to the desired one.

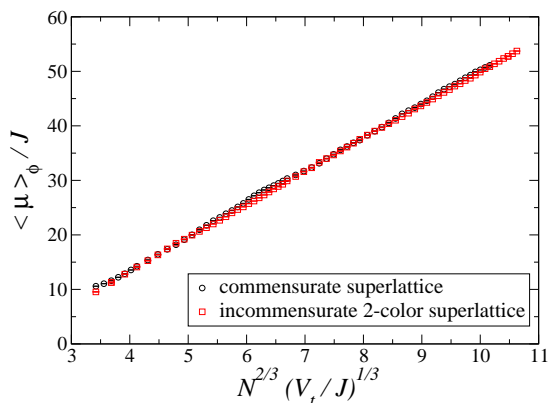


FIG. 5: Phase-averaged chemical potential for the trapped 1d Bose-Hubbard model with a commensurate superlattice potential and with a 2-color incommensurate potential (see text). For both cases  $V_2 = U = 20J$  and  $N = 100$ .

As a summary of the study of one dimensional systems, Table I shows the result of the fit of the various cases considered (no superlattice, commensurate and incommensurate superlattice) to the Ansatz of Eq. (13). We observe that the coefficients  $\gamma_{d=1}$  are essentially all consistent within error bars, as the TF/AL theory would simply predict; more quantitatively, they are all close to the TF/AL prediction  $\gamma_{d=1} = 0.82548\dots$ , which is a remarkable fact given the simplicity of that theory. Moreover the constant terms  $C_{d=1}(U/J, V_2/J)$  appear to be only weakly dependent on the Hamiltonian parameters; in particular, within error bars they appear not to depend on the parameter  $\alpha$  of the superlattice but only on the superlattice strength.

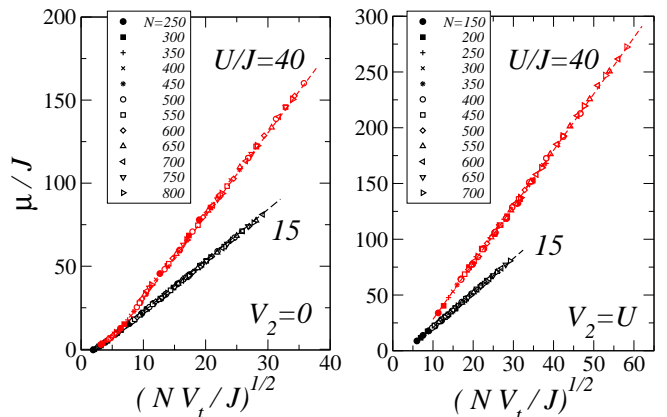


FIG. 6: Chemical potential for the trapped 2d Bose-Hubbard model without (left panel) and with (right panel) a superlattice potential ( $\alpha = 830/1076$  in all spatial dimensions). Dashed lines are fits to the Ansatz Eq. (13).

### 3. $d=2, 3$

Fig. 6 shows the chemical potential for the  $d = 2$  Bose-Hubbard model as numerically determined via quantum Monte Carlo. We have considered the two values  $U/J = 15$  and  $40$  for the interaction: according to the phase diagram of the homogeneous 2d Bose-Hubbard model [45], for the first value the system is always in a superfluid state at all fillings, while for the second value the system experiences Mott insulating phases at fillings  $n = 1, 2, \dots$  upon changing the chemical potential. From Fig. 6 we see that, no matter the phase the system is in, data sets for different particle numbers and varying trapping potentials all collapse onto the same curve when plotted as a function of  $(NV_t)^{1/2}$ , in agreement with the TF/AL prediction, both in absence and in presence of a superlattice potential. For sufficiently high  $N$  and/or  $V_t$  the dependence of  $\mu$  on  $(NV_t)^{1/2}$  is linear and can be well fitted to the Ansatz Eq. (13) giving the results summarized in Table II. It is remarkable that the numerical results for the slope  $\gamma_{d=2}$  are very close to being all numerically consistent with each other, and with the TF/AL prediction  $\gamma_{d=2} = 0.79788$ . On the opposite end, for small  $N$  and/or low  $V_t$ , the local filling can drop to values  $\langle n_i \rangle \leq 1$ , which, in absence of a superlattice, amounts to the onset of a  $n = 1$  Mott plateau for  $U/J = 40$ : this strong lattice commensurability effect, completely neglected in the TF/AL approach in continuum space, is responsible for the deviation of the  $U/J = 40$  results from the linear behavior. As already observed for the  $d = 1$  case [30] the  $\mu$  curve exhibits a crossover to a low-density regime which loses the dependence on the  $U/J$  value, as shown by the merging of the

$U/J$	$V_2$	$\alpha$	$\gamma_{d=2}$	$C_{d=2}$
15	0	-	0.795(3)	-2.1(1)
40		-	0.790(4)	-3.1(1)
15	$U$	830/1076	0.803(6)	-2.6(2)
40		830/1076	0.799(3)	-3.53(8)

TABLE II: Results of the fit of the chemical potential data to the scaling Ansatz Eq. (13) for the 2d trapped Bose-Hubbard model without any superlattice, and with an incommensurate superlattice.

$U/J$	$V_2$	$\alpha$	$\gamma_{d=3}$	$C_{d=3}$
20	0	-	0.801(3)	-3.38(8)
50		-	0.795(5)	-4.55(11)
20	$U$	830/1076	0.812(14)	-4.4(2)
50		830/1076	0.81(5)	-6.3(1.7)

TABLE III: Same as in Table II but for the 3d trapped Bose-Hubbard model.

$U/J = 40$  curve with the  $U/J = 15$  one. In general one does expect all  $\mu$  curves at arbitrary  $U/J$  values to merge onto the same universal curve for a diluted system when  $N, V_t \rightarrow 0$ . Yet a large enough  $U/J$  suppresses double occupancy in a system with filling smaller than unity, so that the actual value of  $U/J$  becomes irrelevant and the system enters the so-called Tonks or hardcore regime: this is the effect responsible for the merging of the  $\mu$  curves at  $U/J = 40$  and  $U/J = 15$  in Fig. 6, well before the regime of extreme dilution is attained (the two curves come close to each other for  $(NV_t)^{1/2}$  values which correspond to a filling  $n \sim 1$  in the trap center). On the contrary, for the  $NV_t$  values we considered, the hardcore regime is not observed in presence of a strong superlattice  $V_2 = U$ , which competes with the repulsion and maintains doubly occupied sites down to the lowest trap fillings we have explored.

To conclude, Fig. 7 shows analogous results for the  $d = 3$  case. We again choose two values of repulsion:  $U/J = 20$ , for which the homogeneous system is superfluid at all fillings [46]; and  $U/J = 50$ , for which the system has Mott insulating regions at fillings  $n = 1, 2, \dots$ . In agreement with the TF/AL prediction, the chemical potential is a homogeneous function of the product  $N^{2/5}V_t^{3/5}$ , and it becomes linear for large enough filling in the trap center ( $n \gtrsim 1$ ); the results of fits to Eq. (13) are summarized in Table III, and show numerical consistency between the estimated slopes  $\gamma_{d=3}$  and the proximity to the TF/AL prediction  $\gamma_{d=3} = 0.81346$ , both in absence and in presence of a superlattice [47]. In the opposite limit of low filling  $n \lesssim 1$ , and in absence of the superlattice, we observe again that the  $\mu$  curves at different  $U/J$  values tend to merge together, which corresponds to the onset of the hardcore regime with suppression of double occupancy.

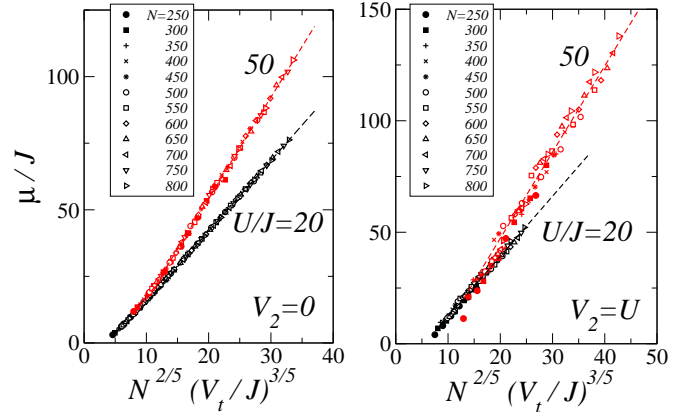


FIG. 7: Chemical potential for the trapped 3d Bose-Hubbard model without (left panel) and with (right panel) a superlattice potential ( $\alpha = 830/1076$  in all spatial dimensions). Dashed lines are fits to the Ansatz Eq. (13).

### C. Quantum Monte Carlo vs. Gutzwiller mean-field results

In the previous section we have seen that the chemical potential of strongly correlated bosonic systems can be described via a modified Thomas-Fermi scaling for sufficiently high densities or sufficiently strong trapping potentials, at which lattice commensuration effects become very weak. On the other hand, lattice effects can be easily taken into account at the classical level via a numerical calculation in the atomic limit, neglecting intersite hopping. Yet such a drastic approximation is going to be unreliable when the hopping energy becomes comparable with the repulsion one, typically when  $2dnJ \sim Un^2$ . Nonetheless, quantum effects can be restored at an approximate level within Gutzwiller mean-field theory, which keeps the cost of numerical calculations at a minimum, while producing predictions which turn out to be in a surprisingly good agreement with those of quantum Monte Carlo.

Gutzwiller mean-field theory assumes a factorized Ansatz for the wavefunction of the many-body system

$$|\Psi\rangle = \otimes_{i=1}^N \left( \sum_{n=0}^{n_{\max}} f_n^{(i)} |n\rangle_i \right) \quad (18)$$

where  $|n\rangle_i$  is a Fock state with  $n$  particles at site  $i$ , and  $n_{\max}$  is a suitable truncation imposed on the local Hilbert space for numerical purposes. Assuming all  $f_n^{(i)}$  coefficients to be real, the expectation value of the Hamiltonian, Eq. (1), on the Gutzwiller Ansatz (GA) wavefunc-

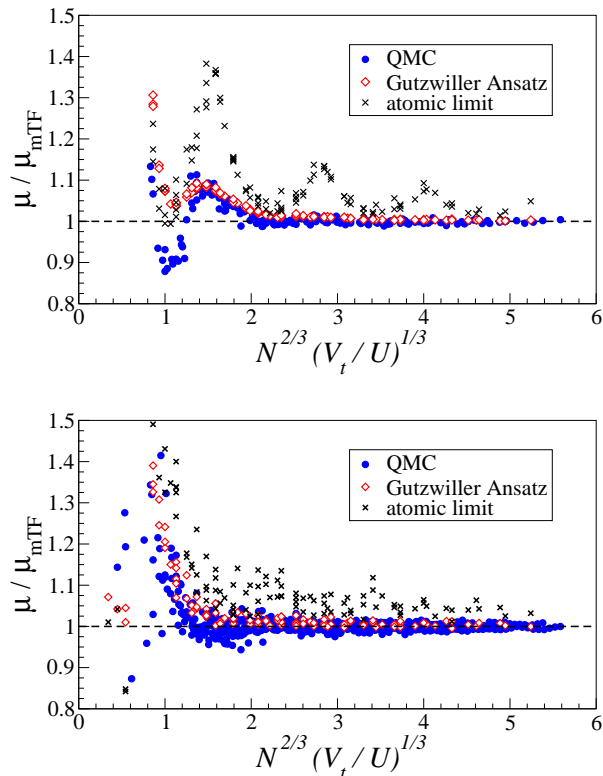


FIG. 8: Chemical potential for the trapped 1d Bose Hubbard model with  $U = 10J$ , as obtained via quantum Monte Carlo, Gutzwiller Ansatz and atomic limit calculations.  $\mu_{\text{mTF}}$  is the modified Thomas-Fermi prediction of Eq. (13) with fitting parameters from Table I. *Upper panel:*  $V_2 = 0$ . *Lower panel:*  $V_2 = U$ ,  $\alpha = 830/1076$ .

tion takes the form

$$\langle \mathcal{H} \rangle = \sum_i \varepsilon_i \quad (19)$$

where

$$\begin{aligned} \varepsilon_i = & - J\gamma_i \sum_n \sqrt{n+1} f_n^{(i)} f_{n+1}^{(i)} \\ & + \sum_n |f_n^{(i)}|^2 \left[ \frac{U}{2} n(n-1) + V_i n \right] \end{aligned} \quad (20)$$

and

$$\begin{aligned} \gamma_i &= \sum_l \sum_n \sqrt{n+1} f_n^{(i+l)} f_{n+1}^{(i+l)} \\ V_i &= V_2 g_i + V_t (r_i - r_0)^2 - \mu. \end{aligned} \quad (21)$$

Here  $\sum_l$  runs on the  $z = 2d$  nearest neighbors in a hypercubic lattice.

The ground state corresponds then to the minimization of the Hamiltonian expectation value with respect

to the  $Nn_{\text{max}}$  coefficients. Instead of proceeding with a full minimization, a usual procedure is to minimize with respect to the local variables  $f_n^{(i)}$  at a site  $i$  while holding fixed the variables at all the other sites. We perform random sweeps over the lattice sites, touching each site once per sweep on average, until convergence is reached – typically less than a hundred sweeps are necessary for convergence. For the Hubbard model under investigation, this leads to a very efficient location of the absolute energy minimum, which can be verified by repeating the minimization starting from a different initial condition.

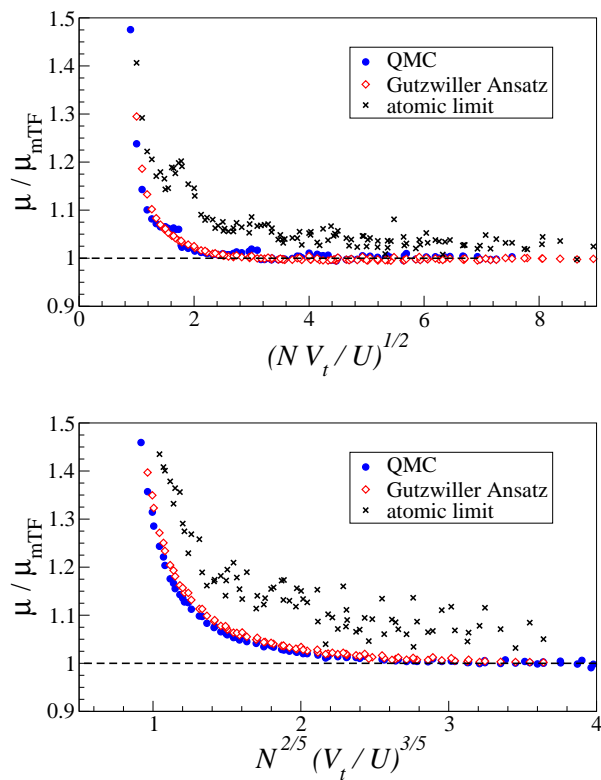


FIG. 9: Chemical potential for the trapped 2d and 3d Bose Hubbard model.  $\mu_{\text{mTF}}$  is the modified Thomas-Fermi prediction of Eq. (13) with fitting parameters from Tables II and III. *Upper panel:*  $d = 2$ ,  $U = 15J$ ,  $V_2 = 0$ . *Lower panel:*  $d = 3$ ,  $U = 20J$ ,  $V_2 = 0$ .

Eq. (18) generally describes a state which does not have a well defined particle number. Given that the minimization of the energy is done in an unconstrained way at each site, we need to adjust the chemical potential  $\mu$  *a posteriori* in order to achieve a desired average particle number  $N = \sum_{i,n} |f_n^{(i)}|^2 n$ , with an analogous procedure to that used with quantum Monte Carlo. Hence this procedure samples the function  $\mu = \mu(V_t, N, J, U, V_2)$  of interest. We use different particle numbers  $N$  and trapping potentials, ranging in the same intervals as those explored in quantum Monte Carlo calculations.

Figs. 8 and 9 compare the results of the GA with those of quantum Monte Carlo calculations for the trapped Bose-Hubbard model in dimensions  $d=1,2$  and 3. Data obtained in the atomic limit  $J = 0$  are also shown as a reference. All data are normalized to the mTF behavior, Eq. (13), attained in the large density / strong confinement limit. The results in the atomic limit are seen to generally overestimate the chemical potential – this is not surprising, given that there is no kinetic energy gain in adding particles to the system in the atomic limit, and hence all the energy gain to balance repulsion has to be provided by the chemical potential. Quite surprisingly, instead, we observe that the mean-field GA accounts very well for the quantum corrections to the atomic limit for *all* system dimensions, and that the chemical potential predicted via the GA is typically less than 4% off with respect to the quantum Monte Carlo prediction. Indeed the GA, while successfully describing the main features of the phase diagram of the Bose-Hubbard model, is not particularly accurate in determining the phase boundaries; given its mean-field nature, it is not quantitatively trustworthy in low dimensions, and its predictions on the location of phase boundaries can be up to 100% off in  $d = 1$ . We find that the GA works equally well even in presence of an incommensurate superlattice potential, despite its inability to describe Anderson localization and Bose-glass physics (data for the case  $d = 1$  are shown in Fig. 8).

A semi-quantitative justification of the success of the GA in predicting the chemical potential of the trapped Bose-Hubbard model can be provided based on LDA. LDA predicts that the total density of the system can be written as

$$N = \sum_i n(\mu_i) \quad (22)$$

where  $\mu_i = \mu - V_t(r_i - r_0)^2$  is the local chemical potential, and  $n(\mu)$  is the density as a function of the chemical potential for the bulk system. The GA might provide a very poor prediction  $n_{\text{GA}}(\mu)$  for the  $n(\mu)$  function of the bulk system, especially in  $d = 1$ , and this might suggest that the global chemical potential  $\mu$  which stabilizes  $N$  particles in the system should be also poorly estimated. Yet what matters in the determination of  $N$  is not the whole  $n(\mu)$  curve, but only its integral. If the difference  $\Delta n(\mu) = n(\mu) - n_{\text{GA}}(\mu)$  oscillates from positive to negative and back, it will be averaged to zero upon integration. This is most likely the case for the Hamiltonian parameters we have considered. As observed *e.g.* in Fig. 8, the most serious problems arise for low  $N$ , which, in a trapped system, implies a chemical potential excursion (from the tails to the center) over which the  $\Delta n$  function has completed only a few oscillations (if any).

## D. Discussion

From the above results we can conclude that the chemical potential for the Bose-Hubbard model in a trap and in a superlattice potential has a simple scaling form as a function of the experimental parameters. On the one hand an accurate determination relies in general on numerics due to the strong interactions in the system; yet we find that the chemical potential appears as a homogeneous function of  $N^{2/(2+d)} V_t^{d/(2+d)}$ , and in particular a linear function thereof for sufficiently high filling in the trap center (typically  $n \gtrsim 1$  in absence of a superlattice, and even lower in presence of a superlattice), and/or weak enough interaction, verifying this way a quantum-modified version of the TF/AL prediction, Eq. (13). Ref. [48] has shown that, under the assumption that LDA holds, one can prove the relationship  $\tilde{\rho} = I_d(\mu/J; U/J)$ , where  $\tilde{\rho}$  is the characteristic density, already introduced above, and  $I_d$  is an unknown function. By inverting the previous relation, this amounts to say that  $\mu$  is a homogeneous function of  $\tilde{\rho}$ , in agreement with our findings. Therefore our results allow to explicitly reconstruct the relation between  $\mu$  and  $\tilde{\rho}$ . This correspondence of our results with the LDA prediction suggests that  $\mu$  is *exactly* a homogeneous function of  $\tilde{\rho}$  if (and possibly only if) LDA is exact. Indeed deviations from perfect homogeneity are seen in our numerical data, for instance in Fig. 8, and they can be attributed in part to numerical uncertainty; in part to the fact that in *any* finite system different  $\mu$  values correspond to the same  $N$  value (which is discretized), so that there is a natural uncertainty on  $\mu$ ; and in part to possible systematic deviations, enhanced in the presence of a rapidly oscillating superlattice. Yet we observe that the homogeneity property is an important simplifying assumption, and it is verified with an accuracy of a few percent in the worst case.

Moreover, in the case of the Bose-Hubbard model without superlattices, Ref. [49] has numerically shown that density profiles (and profiles of other local observables) for trapped bosons having the same characteristic density  $\tilde{\rho}$ , and the same Hamiltonian parameters  $U$  and  $J$ , appear to be invariant up to a rescaling of the space coordinates with the characteristic length  $\eta = \sqrt{J/V_t}$ . This implies that, under rescaling of the coordinates with  $\eta$ , the density at site  $i$ ,  $\langle n_i \rangle = \langle \tilde{n}(\mathbf{r}_i/\eta) \rangle$ , is a unique function of  $\tilde{\rho}$ . At the same time, the local chemical potential,  $\mu_i$ , expressed in terms of rescaled variables, turns out as well to be a unique function of  $\tilde{\rho}$

$$\begin{aligned} \mu_i &= \tilde{\mu}_{\mathbf{r}_i/\eta} = \mu(\tilde{\rho}; U, J) + V_t(r_i - r_0)^2 \\ &= \mu(\tilde{\rho}; U, J) + J[(r_i - r_0)/\eta]^2 \end{aligned} \quad (23)$$

thanks to the result that  $\mu = \mu(\tilde{\rho}; U, J)$ . As a consequence, the results of Ref. [49] suggest that  $\langle \tilde{n}(\mathbf{r}_i/\eta) \rangle$  is a unique function of  $\tilde{\mu}_{\mathbf{r}_i/\eta}$ . In the limit of an infinitely shallow trap,  $V_t \rightarrow 0$  and  $N \rightarrow \infty$  at fixed  $\tilde{\rho}$ , the dependence of  $\langle \tilde{n}(\mathbf{r}_i/\eta) \rangle$  on  $\tilde{\mu}_{\mathbf{r}_i/\eta}$  must reproduce the de-

pendence of the bulk density on the chemical potential,  $n(\mu)$ . Hence the unique function relating  $\langle \hat{n}(\mathbf{r}_i/\eta) \rangle$  to  $\hat{\mu}_{\mathbf{r}_i/\eta}$  must be identical with that of the bulk limit. As a consequence, the invariance of the density profiles (and, with the same reasoning, of any other local observable in the trap) under rescaling with  $\eta$  implies that the LDA is exact. It is trivial to show that the exactness of the LDA implies the invariance of local quantities under rescaling with  $\eta$ . Hence we can conclude that the scale invariance of trapped systems at fixed characteristic density is exact *if and only if* LDA is exact. Yet, even when LDA is not exact, the system might display scale invariance with a better accuracy than that of LDA, as shown numerically in Ref. [49] in the case of density fluctuations and local compressibility.

At the experimental level, the above results reveal the possibility of controlling the chemical potential in the trapped system by: 1) controlling the trapping frequency at fixed particle number, or viceversa 2) controlling the particle number at fixed trap strength, or 3) controlling both simultaneously. Hence the present experimental setups have direct access to the measurement of phase diagrams of strongly correlated bosons in the *grand-canonical* ensemble at variable chemical potential. Most noticeably, an accurate knowledge (within a few percent) of the zero-temperature chemical potential as a function of the Hubbard Hamiltonian parameters can be obtained with little numerical effort via the mean-field Gutzwiller Ansatz, namely without fully solving numerically the many-body problem. This aspect is to be contrasted with the case of accurate thermometry of strongly correlated bosons, which at the moment can be reliably assessed only via exhaustive ab-initio simulations [17, 18].

#### IV. TRAP-SQUEEZING PROTOCOL

The previous section has shown how the chemical potential of a trapped system is simply controlled by the number of particles  $N$  and by the trapping potential  $V_t$ . Indeed recent experiments have probed the compressibility of fermions loaded in optical lattices by varying the trapping potential [31] or the atom number [50, 51], although the explicit relation between the experimental parameter and the chemical potential was not known for that system. In the experiments, the atom number is typically subject to significant fluctuations due to shot noise of order  $\sqrt{N}$ , as well as to other systematic effects. On the contrary the trapping potential  $V_t$  can be controlled on a much finer scale via the application of a dipolar trap along the spatial direction of interest, namely by shining  $d$  red-detuned running laser waves onto the sample to control the confinement in  $d$  spatial dimensions (this is sketched in Fig. 10 for the case of variable one-dimensional confinement). The dipolar trap adds up to the confining (anti-confining) potential given by the overall gaussian intensity profile of the red-detuned (blue-detuned) optical lattice, and it gives the possibility of

varying the trap strength  $V_t$  *independently* of the Hamiltonian parameters  $U$ ,  $J$ ,  $V_2$ , offering in this way the possibility of simulating the Bose-Hubbard Hamiltonian in a variable trapping potential [31, 52].

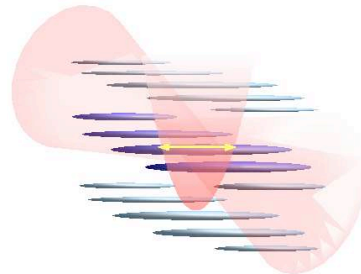


FIG. 10: Schematic view of the confinement control on the longitudinal direction in a set of one-dimensional tubes.

In the remainder of the paper we hence focus on the proposal of extracting the phase diagram of the Bose-Hubbard model in the grand-canonical ensemble by controlling the chemical potential of the system via trap-squeezing and at fixed particle number. Two fundamental issues are addressed in the next subsections concerning the experimental feasibility of this proposal: 1) we discuss the fundamental difficulty in achieving adiabatic trap-squeezing once the particles are loaded in the optical lattice; 2) hence we propose a simple loading sequence which overcomes this difficulty, and which allows to control the particle number in the central tubes/layers in the case of  $1d/2d$  confinement.

##### A. The adiabaticity issue

Optical lattice experiments have revealed the unique possibility of tuning the Hamiltonian parameters in real time, *e.g.* via changing the intensity of the standing wave which controls the  $U/J$  parameter [53]. A fundamental issue raised by such real-time control is the possible generation of excitations in the system by a non-adiabatic change of the Hamiltonian parameters. This becomes particularly dramatic when the parameter change implies the crossing of a quantum critical point, at which the gap over the ground state vanishes, leading to efficient Landau-Zener tunneling [54]. Similarly to the change in the optical lattice strength, a change in the dipolar trapping strength can also lead to quantum phase transitions, driven this time by the chemical potential, and hence it is subject to adiabaticity issues. In fact adiabaticity is even more problematic in the case of trap squeezing: regarding the center of the trap as the system, and the trap periphery as the particle reservoir (as mentioned in the Introduction), the process of transfer of particles between system and reservoir under trap squeezing might be pathologically slow if the particles are strongly localized in one part or the other, due to strong interactions

in presence of an optical lattice or to (quasi-)disorder potentials.

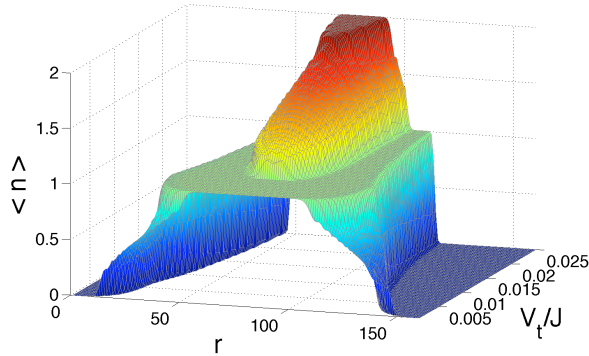


FIG. 11: Density profile as a function of trap strength for the Bose-Hubbard model with  $N = 100$  particles and with  $U = 20/J$ , as resulting from an extended fermionization calculation (see text and Appendix A).

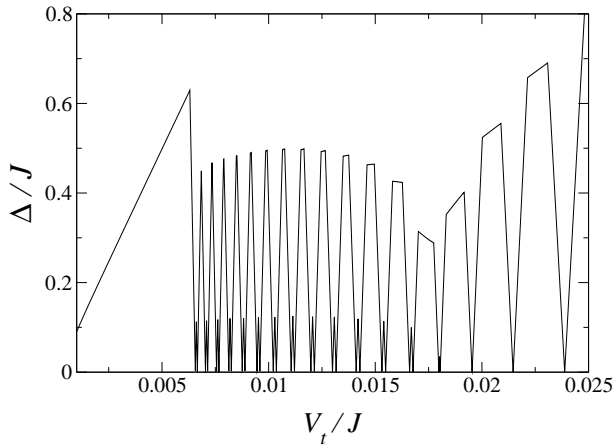


FIG. 12: Lowest energy gap  $\Delta$  as a function of trap strength for the Bose-Hubbard model. Parameters as in Fig. 11

We exemplify the above discussion in the case of lattice *hardcore* bosons, for which the exact many-body spectrum can be calculated exactly via Jordan-Wigner diagonalization [43], in the case of density  $n \leq 1$  on each site. The fermionization approach can be extended to the case  $n > 1$  [55] under the condition of having a well developed layer-cake structure of the density profile (see Appendix A for a detailed discussion). Fig. 11 shows the evolution of the density profile upon trap squeezing for the trapped Bose-Hubbard model with  $U = 20J$  and with  $N = 100$  particles, as obtained via extended fermionization. For the chosen range of trap strengths, we observe

that the system goes from a Mott-insulating phase with  $n = 1$  particles in the trap center to a superfluid phase with  $1 < n < 2$  and finally to a Mott-insulating phase with  $n = 2$  particles. In particular, the “local transition” from Mott insulator to superfluid in the trap center at fixed particle number is exclusively due to the redistribution of particles from states in the wings of the trap to states in the center. The states in the trap periphery are localized by the joint effect of the strong repulsion exerted by the particles in the trap center and of the confining potential. On the other hand the states in the trap center are localized by the confining potential over a length scale which is well below the width of the atomic cloud. Hence the spatial overlap between such states is negligible, and they are separated by a high potential barrier - which is represented by the atoms forming the  $n = 1$  Mott plateaus. This implies that the tunnel splitting between the states in the center and the states in the wings can be extremely small, and hence the ground state can become nearly degenerate with the first excited state. This is indeed revealed by the direct investigation of the lowest energy gap, which, within the extended fermionization approach, is estimated as the lowest particle-hole excitation energy for the spinless fermions, and it is shown in Fig. 12. We observe that such a gap goes to a value very close to zero [56] when the first particles move from the trap wings to the trap center, corresponding to the occurrence of an insulator-to-superfluid transition in the trap core. The gap shows as many dips as particles transferred to the center, revealing the tightly avoided level crossings corresponding to the particle redistribution - more precisely, each deep minimum of the  $\Delta$  vs.  $V_t$  curve corresponds to the successive migration of two particles from the wings to the center, because such particles occupy states which are nearly degenerate symmetric/antisymmetric superpositions of localized states on the two opposite wings of the trap). Hence this succession of tightly avoided level crossings makes adiabatic trap squeezing essentially impossible in presence of Mott-insulating regions, as squeezing times which are several orders of magnitude bigger than the typical tunneling time ( $\sim$ ms) would be required.

As a second example we consider the case of  $N = 50$  hardcore bosons in an incommensurate superlattice potential Eq. (3) with  $\alpha = 830/1076$  (as experimentally realized in Ref. 22) and  $V_2 = 20J$ . Such a potential is known to lead to Anderson localization of all single-particle states for  $V_2 > 4J$  [57, 58]. In this case standard fermionization provides the exact spectrum, and in particular the lowest energy gap as a function of the trap strength, as shown in Fig. 13. We observe that the gap can become extremely small, this time due to the quasi-degeneracy of Anderson localized states which are spatially well separated, so that the tunnel splitting between them is very small.

Hence from these two examples we can conclude that either strong repulsion induced by the optical lattice, or a (pseudo-) disorder potential, give rise to localized single-

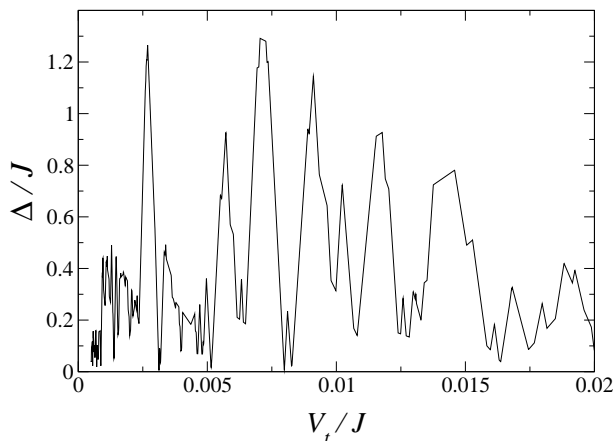


FIG. 13: Lowest energy gap  $\Delta$  as a function of trap strength for  $N = 50$  hardcore bosons in an incommensurate superlattice ( $\alpha = 830/1076$ ) of strength  $V_2 = 10J$ .

particle states, which become quasi-degenerate upon changing the trap frequency. This leads to a very efficient Landau-Zener tunneling which essentially makes adiabatic trap squeezing impossible. Although the results shown here are obtained for a one-dimensional system, their underlying mechanism is quite general and applies to higher dimensions as well. Hence we can generally conclude that adiabatic trap-squeezing for a system of particles loaded in a strong optical (super)lattice is virtually impossible. Luckily the statement of the problem already contains in itself the solution: trap squeezing has to be performed *before* loading the particles in the optical (super)lattice, namely when the particles still enjoy their full mobility, so that they can adiabatically follow the variation in the trapping potential. In the case of spatially anisotropic optical lattices, discussed in the next subsection, this consideration applies to the loading of the particles in the optical lattice along the spatial dimensions in which the particles are more weakly confined.

### B. Trap squeezing protocol for low-dimensional systems

In the case of spatially anisotropic optical lattices, allowing to simulate the  $1d$  or  $2d$  Bose-Hubbard model [21, 59], the control of the chemical potential can be achieved by trap squeezing along the spatial dimensions of interest, namely along the tubes in  $1d$ -anisotropic optical lattices and along the layers in  $2d$ -anisotropic ones. Yet, if the strength of the trapping potential is changed before confining the atoms in tubes or in layers, the final atomic population present in the tubes/layers will be significantly affected, so that one violates the condition of working at fixed particle number in the low-dimensional elements (tube or layer) of the system, and in partic-

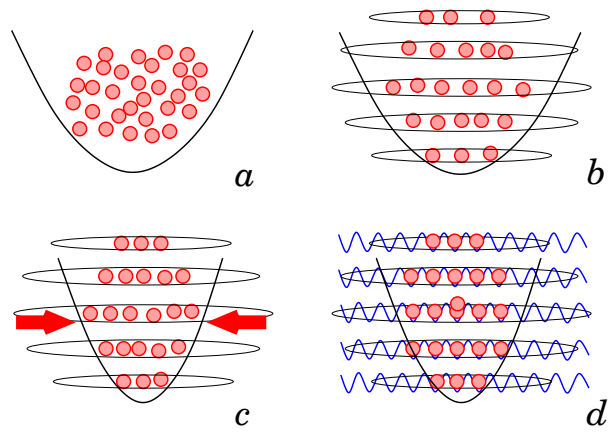


FIG. 14: Sketch of the proposed loading and squeezing protocol of atoms in a spatially anisotropic optical lattice. The description of the various stages is presented in Sec.IV B.

ular in the central ones. The problem of guaranteeing at the same time the control on the particle number in the tubes/layer and adiabatic trap squeezing can be easily solved by considering the following loading protocol, sketched in Fig. 14:

a) Particles are initially trapped in a dipolar trap or a magneto-optical trap (MOT) at fixed strength;

b) A deep one-dimensional/two-dimensional optical lattice is then ramped up, defining layers/tubes in which the atoms are still moving in continuum space. For a given initial atom number  $N$  the overall trapping potential (dipolar trap or MOT plus the optical lattice beam profile) uniquely defines the populations in each tube/layer. These populations remain essentially fixed for the rest of the experiment, thanks to the deep optical lattice. Given that the atoms are still in the weakly interacting regime, we can determine these populations via the Thomas-Fermi approximation – the results are given by Eqs. (B6) and (B9) in Appendix B);

c) Varying the dipolar trapping along the tube/layer dimensions gives rise to trap squeezing, which can be easily kept adiabatic for weakly interacting particles [60];

d) At this stage the optical lattice can be adiabatically ramped up along the tubes/layers, finally realizing a  $1d/2d$  Bose-Hubbard Hamiltonian at a given particle number and in a given longitudinal trapping potential.

## V. IMAGING TECHNIQUES

The two previous sections have discussed how to achieve full control on the chemical potential of the Bose-Hubbard model realized in optical lattice experiments via the control on the trapping potential at fixed particle number. As discussed in Section II, the overall chemical potential of the trapped system corresponds in particular to the local chemical potential at the trap center: hence, getting access to the average central density in

the trap as a function of the chemical potential gives the possibility of extracting experimentally the density curve of the *bulk* Bose-Hubbard model in the grand-canonical ensemble and hence its compressibility.

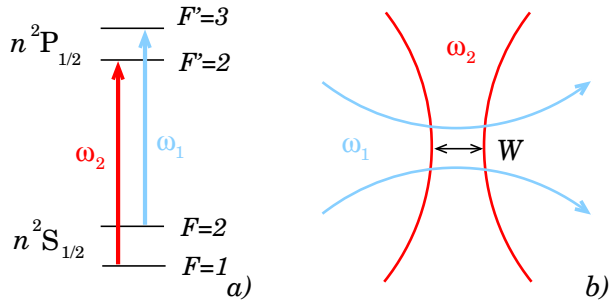


FIG. 15: Sketch of the proposed imaging protocol for alkali atoms. A repumping ( $\omega_2$ ) and a cooling ( $\omega_1$ ) beam are tightly focused on the center of the trap, and they are crossed so as to overlap in a region of width  $\approx W$  (minimal beam waist) in all spatial directions. This setup realizes a spatially-resolved optical cycling transition.

As it will be further seen in the next Sections, measuring an average central density which mimics closely the one of the bulk system requires imaging the atomic cloud over a typical length scale of 10-20 lattice sites in each spatial direction for typical atom numbers and trapping frequencies used in current experiments, corresponding to a spatial resolution of  $\sim 5 - 10 \mu\text{m}$ . To achieve this resolution, a possible technique is given by spatially resolved fluorescence imaging for atoms (see Fig. 15). In the case of alkali atoms initially prepared in an  $F = 1$  hyperfine state of the  $n^2S_{1/2}$  level, a repumping beam, resonant with the transition to an  $F' = 2$  state of the  $n^2P_{3/2}$  level, optically pumps the atoms into an  $F = 2$  state [61]; a second beam resonant with the  $F = 2 \rightarrow F' = 3$  transition (cooling beam) is then used to image the atoms. If the two beams are tightly focused to a beam waist of  $\sim 5 - 10 \mu\text{m}$  and are perpendicular to each other such that they meet at the focal point, they selectively image atoms in a region of space of the desired size. Typical optical lattice experiments have  $n > 1$  particles per lattice site in the trap center, so that imaging a central region with  $10^3 - 20^3$  lattice sites involves imaging at least as many atoms, which is possible over a time  $\lesssim 100$  ms (see *e.g.* Ref. 62). Before imaging, the optical lattice could be rapidly increased to the maximum height in order to freeze the atomic cloud profile during the successive imaging time.

The proposed imaging technique has the advantage of being generally compatible with common atom trapping setups based on magneto-optical or dipolar traps, and to require only an intermediate imaging resolution. On the other hand, ultra-high resolution optics has given access to few-site/few-atom or even single-site/single-atom imaging, in a variety of very recent experiments [25–29]. This level of resolution far exceeds the one required by

our present proposal. An alternative technique for the indirect extraction of the local density in the trap consists in the high resolution *in-situ* imaging of the atomic cloud density integrated along the line of sight, from which the full three-dimensional atomic distribution is reconstructed via inverse Abel transformation [63, 64]. Given the diversity of techniques mentioned above, we are confident that the extraction of the local density properties in selected regions of the trap will become an experimental routine in the near future.

After the *in situ* imaging stage, turning off all trapping potentials and imaging the expanded cloud gives access to the total number of atoms. This piece of information is fundamental to *post-select* the measurements with a given total atom number  $N$ , which corresponds to the desired value of the chemical potential to be realized in the experiment. Strictly speaking, once the calibration curve relating  $\mu$  to  $N$  is known, the final measurement of the particle number has only the role of assigning the measurement of the central density to the proper place in the grand-canonical phase diagram of the bulk system. Hence one can regard the fluctuations in the total particle number  $N$  as a source of random sampling of the  $\mu$  axis in that phase diagram. In this perspective, all measurements give useful information, provided that particle number fluctuations are not bringing the chemical potential  $\mu$  too far from the region of interest in the phase diagram.

## VI. APPLICATIONS: PHASE DIAGRAM OF THE 1d BOSE-HUBBARD MODEL

As a first application of trap squeezing, we investigate the ground-state phase diagram of the one-dimensional Bose-Hubbard model. We consider the situation of  $N = 100$  bosons trapped in the central tube of a strongly anisotropic optical lattice [21], and addressed with spatially resolved imaging described in the previous section. We present quantum Monte Carlo results for the central properties in the trap, as well as for the global time-of-flight properties. The chemical potential  $\mu$  is adjusted so that the ground state of the grand-Hamiltonian, Eq. 4, has the desired number of bosons.

### A. Central compressibility

Investigating the phase diagram of the Hubbard model via trap squeezing implies that the superfluid-insulator transitions that one can probe are accessed via a variation of the chemical potential, namely they are of the commensurate-incommensurate kind in a system without disorder. Such transitions have the advantage of being very sharp, as they are characterized roughly speaking by the appearance (or disappearance) of a superfluid component in the system, induced by doping particles or holes into a Mott insulating state at integer filling. The

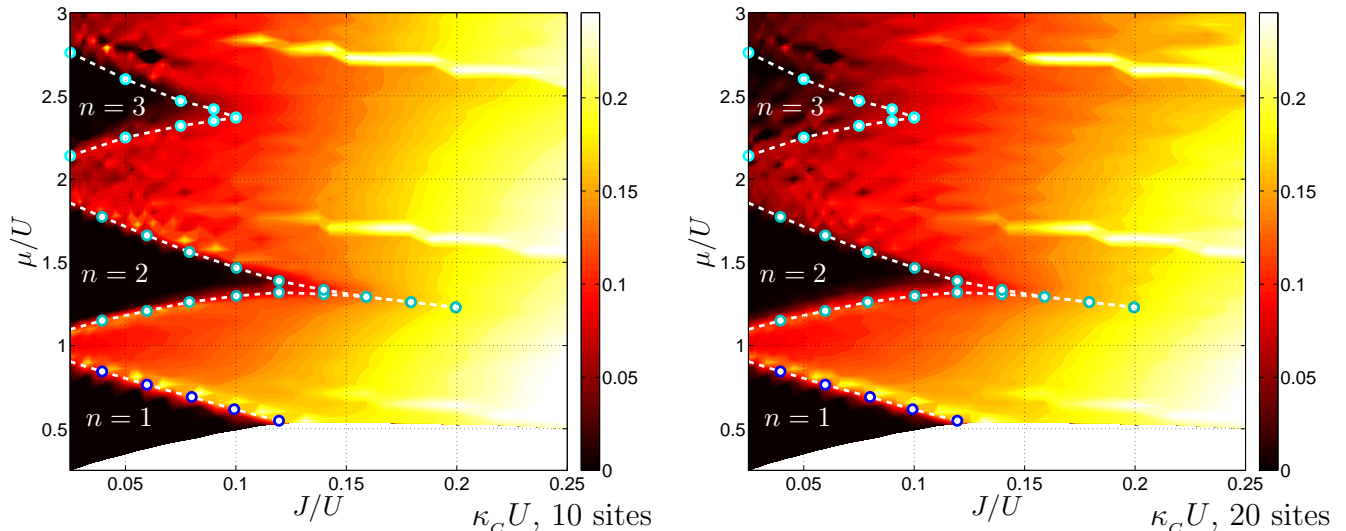


FIG. 16: Central compressibility  $\kappa_C = \partial n_C / \partial \mu$  (in units of  $U^{-1}$ ) of  $N = 100$  bosons under variable trapping frequency. The central density  $n_C$  is obtained by imaging over 10 sites (left panel) and 20 sites (right panel). The white curves report the boundary lines between superfluid and Mott-insulating phases as determined in Ref. 40 (for the  $n = 1$  and  $n = 2$  lobe) via density-matrix renormalization group, and independently in this work (for the  $n = 3$  lobe) via quantum Monte Carlo.

superfluid-insulator transition can be completely characterized by the compressibility  $\kappa = \partial n / \partial \mu$ , which, similarly to the superfluid density, is identically zero in the Mott-insulating phase and finite in the superfluid phase, for all spatial dimensions. In particular the compressibility has quite a sharp variation at the transition in low-dimensional systems. Indeed its critical scaling with system size  $L$  obeys the law  $L^{d-z}$  [8] where  $z = 2$  is the dynamical critical exponent; hence, for  $d = 1$ , it jumps from a value diverging linearly with system size to zero at the transition point (while in  $d = 2$  the jump takes place from a value diverging logarithmically with the system size). This very sharp feature makes it possible to detect the transition unambiguously even on a small system size, which is effectively the case here. In the following we deliberately limit our attention to the  $n > 1$  region of the phase diagram, as this is a typical situation in the experiments.

We focus our attention on the behavior of the *central compressibility*,

$$\kappa_C = \frac{\partial n_C}{\partial \mu} \quad (24)$$

corresponding to the response of the density in the central region  $C$  to a variation of the chemical potential, driven exclusively by a change in the trapping potential (which leaves the parameters  $J$  and  $U$  unchanged). Upon choosing a sufficiently narrow central region  $C$  satisfying the condition of Eq. 7, the central density is supposed to reproduce closely the behavior of the compressibility in the bulk system. Fig. 16 shows indeed that this is the case. In fact we observe that the central compressibility jumps from a finite value to zero for critical values of

the chemical potential which reproduce closely the shape of the Mott-insulating lobes of the *bulk* phase diagram of the  $1d$  Bose-Hubbard model. (The Mott insulating boundaries for the bulk system have been determined in Ref. [40] via density-matrix renormalization group for the  $n = 1$  and  $n = 2$  lobes, while we have determined the  $n = 3$  lobe via quantum Monte Carlo). Remarkably, upon doubling the central region  $C$  from 10 to 20 sites (namely halving the resolution of the imaging in the experiment), the main features of the reconstructed phase diagram are only slightly altered, at least for what concerns the lobes  $n = 1, 2$ . This shows the robustness of the proposed approach under realistic experimental conditions. An interesting phenomenon to be observed in Fig. 16 is the "blue shift" (towards higher chemical potentials) of the  $n = 2$  and  $n = 3$  Mott lobes predicted by the vanishing of  $\kappa_C$  with respect to what is observed in a bulk system. This shift can be easily understood as a result of the finite width of the imaging region and as an effect of the finiteness of the central region exhibiting bulk physics, and, as we will discuss, it can be corrected for systematically.

*Blue shift of the lower lobe boundaries.* The lower lobe boundaries are associated with a SF-MI transition induced by an increase of the chemical potential above a lower critical value  $\mu_c^{(l)}(J/U)$ . A chemical potential  $\mu > \mu_c^{(l)}$  forces the atom density to an integer value, for which a Mott gap opens if  $J/U < (J/U)_c$  corresponding to the lobe tip. When this phenomenon occurs in the center of the trap, the MI region which appears at first is extremely narrow in space (see Fig. 17(a) for a sketch). Indeed it extends over a region of width  $\Delta r$  such that

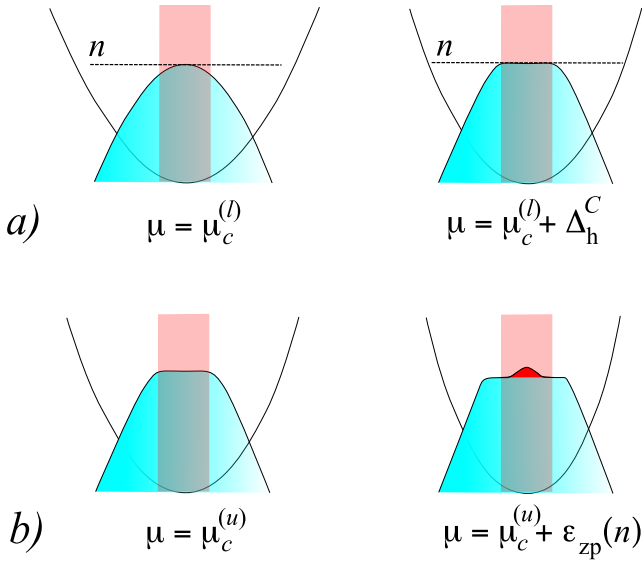


FIG. 17: Mechanisms of blue shift of the Mott lobes obtained from the central compressibility. *a*) At the lower critical chemical potential  $\mu_c^{(l)}$  a Mott region only forms on the central site, and one needs an increase of the chemical potential by a term  $\Delta_h^C$  to establish a Mott phase throughout the imaging region (pink-shaded). *b*) At the upper critical potential  $\mu_c^{(u)}$  of the bulk system, the trapped system has not yet developed a superfluid core, because of the additional zero-point energy  $\varepsilon_{zp}(n)$  due to trapping in the harmonic oscillator potential. Only when the chemical potential reaches the blue-shifted value  $\mu_c^{(u)} + \varepsilon_{zp}(n)$ , the first particle of the superfluid core appears (marked in red).

the chemical potential modulation due to the trap over this region is lower than the MI hole gap  $\Delta_h$ , namely  $V_t(\Delta r/2)^2 \approx \Delta_h$ . The central compressibility detects the appearance of an incompressible MI phase in the trap center only when  $\Delta r$  reaches the size  $|C|$  of the imaging region, namely for a critical bulk gap  $\Delta_h^C \approx V_{t,C}(|C|/2)^2$ . Here  $V_{t,C}$  is the trapping potential corresponding to the effective chemical potential  $\mu(V_{t,C}, N, J, U)$  at which the hole gap takes the value  $\Delta_h^C$ . This chemical potential is simply given by  $\mu_c^{(l)} + \Delta_h^C$ . This implies that, for a strong confinement  $V_t$ , as that required to obtain  $n = 2$  or  $n = 3$  MI lobes in the system, one observes the onset of a MI phase for a blue-shifted critical chemical potential

$$(\mu_c^{(l)})' = \mu_c^{(l)} + \Delta_h^C. \quad (25)$$

Remarkably this shift depends exclusively on experimentally known parameters  $V_t$  and  $|C|$ , so that one can correct *a posteriori* for it when determining the phase diagram experimentally.

*Blue shift of the upper lobe boundaries.* The upper lobe boundaries are associated with a MI-SF transition, induced by an increase of the chemical potential. Reaching an upper critical value  $\mu_c^{(u)}$ , the chemical potential closes the Mott gap of the MI with  $n$  particles per site,

and it therefore adds the first particles on top of the Mott insulator. In a bulk system these particles are essentially added in a  $k = 0$  state, and they undergo condensation. In a trap, the corresponding phenomenon would be the appearance, induced by trap squeezing, of the first particle over the central Mott plateau with  $n$  particles per site (see Fig. 17(b)). At variance with the bulk case, these particles are not fully delocalized, but they still feel the overall trapping potential - hence they have a residual zero-point energy, due to the confinement in the trap. To estimate this shift in the zero point energy, we can proceed in the spirit of the extended fermionization approach [55], (see Sec. IV and Appendix A, and use the approximation of representing the extra particle added in the trap center as moving on an inert background at fixed density  $n$ , whose only effect is to increase the hopping amplitude of the particle from  $J$  to  $J(n+1)$ ). Hence the zero point energy can be estimated from the solution of a harmonic oscillator of effective mass  $m^* = \hbar^2/[2J(n+1)]$  and frequency  $\hbar\omega = \sqrt{4(n+1)V_t J}$ . This estimate is valid as long as the width of the central MI plateau is larger than the width of the ground state of the harmonic oscillator, namely  $\sigma = [J(n+1)/V_t]^{1/4}$ . Hence the shift in zero-point energy due to confinement is  $\varepsilon_{zp}(n) = \hbar\omega/2 = \sqrt{(n+1)V_t J}$ . This leads to a shift in the critical chemical potential needed to “dope” a particle onto the central MI plateau with respect to that needed in a bulk system; as a consequence, the upper critical chemical potential  $\mu_c^{(u)}$  measured by the central compressibility is blue-shifted as

$$(\mu_c^{(u)})' = \mu_c^{(u)} + \varepsilon_{zp}(n). \quad (26)$$

Similarly to what observed for the lower lobe boundary, one can correct *a posteriori* for this shift using the experimental parameters, and hence reconstruct the bulk value of  $\mu_c^{(u)}$ .

Fig. 18 shows the lower and upper critical chemical potentials of the  $n = 2$  MI lobe, as extracted from the vanishing of the central compressibility of  $N = 100$  bosons imaged over the central 20 sites, and compared with the numerically exact results of Ref. 40. The blue shift of the lower critical chemical potential is quite sizable, but it is seen to be very well corrected for by the prediction of Eq. (25). The blue shift of the upper critical chemical potential is instead much weaker, in agreement with the prediction of Eq. (26). This shows that trap squeezing allows to reconstruct quite accurately the quantum phase transition lines of the Bose-Hubbard model, even in the case of a coarse imaging of a central region of  $\sim 20$  sites in the trap center.

Trap squeezing supplemented with imaging over  $|C|$  sites can reliably detect MI behavior only as long as the MI plateau occurring in the trap center can reach the same width as that of the central  $C$  region: this condition guarantees that  $(\mu_c^{(l)})' < (\mu_c^{(u)})'$ , namely that, upon increase the chemical potential, the (blue-shifted) lower chemical potential is reached before a new super-

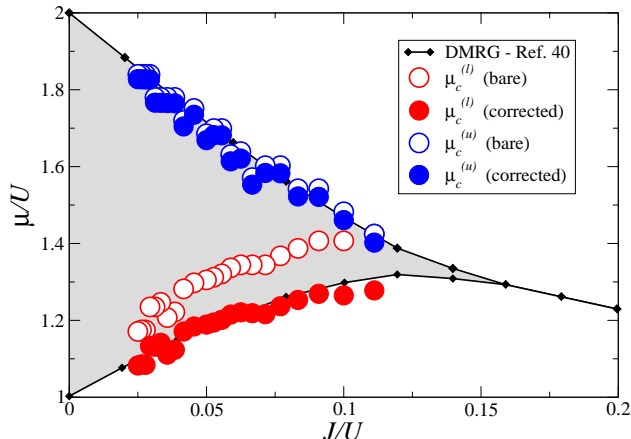


FIG. 18:  $n = 2$  Mott lobe of the  $1d$  Bose-Hubbard model as determined by trap squeezing of  $N = 100$  bosons, imaged over the central 20 sites. The open circles correspond to the bare values of the lower and upper critical chemical potentials extracted from the vanishing of the central compressibility for  $|C| = 20$  (Fig. 16); the closed circles correspond to the values corrected for blue shift, according to Eqs. (25) and (26). The correction leads to a very good agreement with the DMRG results of Ref. 40.

fluid core forms. The MI region can no longer be reliably observed if  $V_t$  reaches the value  $\bar{V}_t$  satisfying the condition  $(\mu_c^{(l)})' = (\mu_c^{(u)})'$ , namely

$$\bar{V}_t (|C|/2)^2 - \sqrt{(n+1)\bar{V}_t J} = \mu_c^{(u)} - \mu_c^{(l)} = \Delta_{\text{ph}} \quad (27)$$

where  $\Delta_{\text{ph}}$  is the particle-hole gap of the Mott insulating phase. The above condition gives

$$\bar{V}_t = \frac{\Delta_{\text{ph}}}{R^2} - \frac{\sqrt{(n+1)J\Delta_{\text{ph}}}}{R^3} + \frac{(n+1)J}{2R^4} + \mathcal{O}\left(\frac{1}{R^5}\right) \quad (28)$$

where  $R = |C|/2 \gg 1$ . The merging of the blue-shifted lower Mott lobe boundary with the upper one is seen to occur *e.g.* in Fig. 18 for  $J/U \gtrsim 0.12$ . To be able to observe the tip of the Mott lobe via trap squeezing, it would be necessary to increase the total particle number so that  $V_t$  can be decreased below  $\bar{V}_t$ , maintaining the same chemical potential in accordance with Eq. (13).

So far we have focused our discussion on the spectral properties associated with the compressibility. In the following we will also discuss the evolution of the coherence properties under trap squeezing, as an alternative tool to investigate the phase diagram of the system.

## B. Time-of-flight observables and condensate compressibility

At variance with diagonal observables such as density and compressibility, which can be measured locally, the phase coherence properties, encoded in the momentum distribution, are generally measured at the global level. We define the momentum distribution as

$$n(k) = \frac{1}{N} \sum_{ij} e^{ik(r_i - r_j)} \langle a_i^\dagger a_j \rangle. \quad (29)$$

where the normalization to the boson number  $N$  is chosen so as to account for the actual spatial extent of the cloud [65]. The momentum distribution is probed via time of flight measurements, by collecting the interferogram of the matter wave emitted from all sites of the optical lattice. Given the strong inhomogeneity of the trapped system, one can suspect that the momentum distribution of a trapped gas is generally not a faithful portrait of the corresponding distribution of a homogeneous system with the same global chemical potential. Yet some remarks are in order. For any given tolerance  $\epsilon$ , one can select a central region  $C$  satisfying Eq. (7), and a complementary region  $\bar{C}$ . Hence the momentum distribution can be decomposed into three contributions, two of which involve the central region  $C$

$$n(k) = n_C(k) + n_{C,\bar{C}}(k) + n_{\bar{C}}(k) \quad (30)$$

where

$$n_{C(\bar{C})}(k) = \frac{1}{N} \sum_{i,j \in C(\bar{C})} e^{ik(r_i - r_j)} \langle a_i^\dagger a_j \rangle \quad (31)$$

and

$$n_{C,\bar{C}}(k) = \frac{1}{N} \left( \sum_{i \in C, j \in \bar{C}} + \sum_{i \in \bar{C}, j \in C} \right) e^{ik(r_i - r_j)} \langle a_i^\dagger a_j \rangle \quad (32)$$

We would like to argue in the following that the behavior of the global momentum distribution is strongly dependent on the contribution  $n_C(k)$  from the central region. Indeed the central region of the trap is the only *simply* connected region, which implies that the pairs of sites  $(ij)$  associated with this region are the ones at the shortest mutual distance  $|r_i - r_j|$ . This latter topological aspect has strong consequences on the coherence properties of the global system. Indeed one can envision in general two situations: 1) If the central region  $C$  is locally in a SF state, its coherence properties are going to give the dominant contribution to the sum of Eq. (29), because  $n_C(k)$  contains the largest number of strongly correlated pairs  $(ij)$  at short distance; moreover if the wings are SF too, the central region will also contribute with the  $n_{C,\bar{C}}(k)$  term, which generally dominates over  $n_{\bar{C}}(k)$  because the central region is at a higher density than its complement  $\bar{C}$ . 2) If the central region is in a local MI phase, extending over a region of linear size  $\sim R_C$ ,

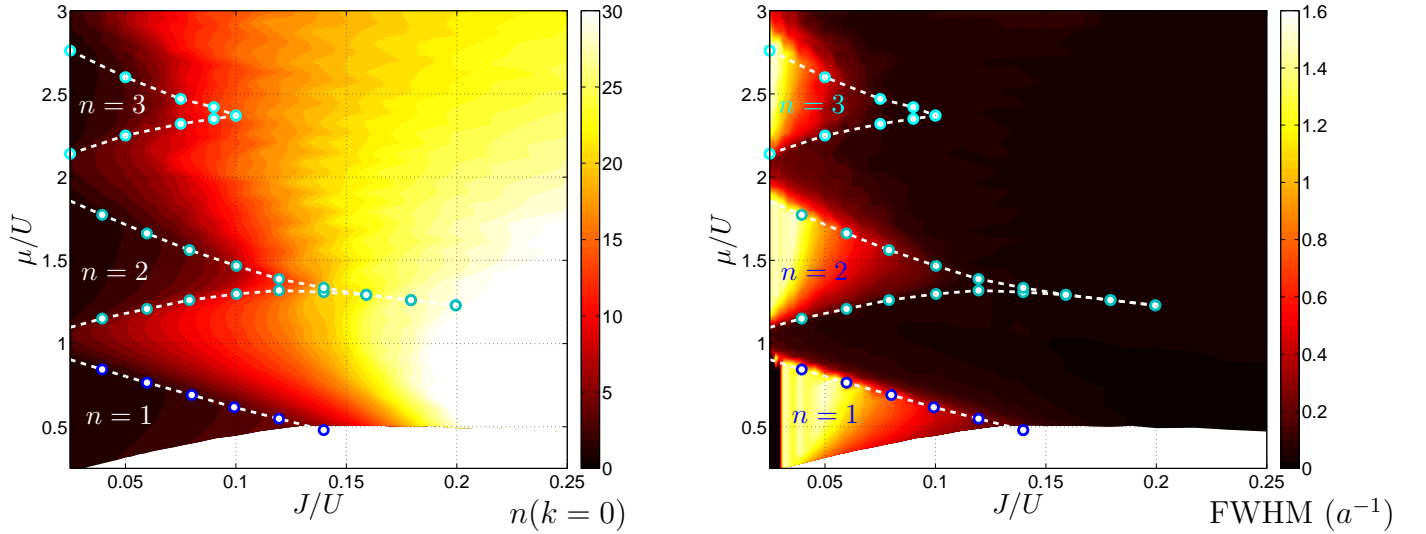


FIG. 19: Evolution of time-of-flight observables for  $N = 100$  bosons under variable trapping frequency. The left panel depicts the condensate number  $n_{k=0}$ , and the right panel the full width at half maximum (FWHM) of the momentum distribution  $n_k$ , in units of  $a^{-1}$  where  $a$  is the lattice spacing.

there might still be a SF halo in the region  $\bar{C}$ , but it will give a weak contribution to the  $n(k)$  because the pairs of sites ( $ij$ ) involved in  $n_{\bar{C}}(k)$  are separated by a distance  $\sim R_C$ , and sites separated by the central MI core are very weakly correlated, given that particles cannot coherently propagate across  $C$ . An equivalent statement to the latter one is that in a  $d$ -dimensional system the SF halo surrounding a MI region is effectively quasi- $(d-1)$ -dimensional, and consequently it has reduced coherence properties, due to the enhanced role of quantum fluctuations in lower dimensions. Hence it is reasonable to believe that the momentum distribution mainly reflects the coherence properties of the central  $C$  region, at least for one- and two-dimensional systems.

Fig. 19 shows the height of the  $k = 0$  peak and the full width at half maximum (FWHM) of the  $n(k)$  in a system of  $N = 100$  bosons under trap squeezing control of the chemical potential, and for various optical lattice depths. Plotting these quantities on the  $(J/U, \mu/U)$  plane, one sees that sharp drops in the global coherence of the trapped system are observed close to the SF-MI boundary lines of the bulk phase diagram of the Bose-Hubbard model. As in the case of the global compressibility, for high enough density the sharpest features in the coherence properties are observed for blue-shifted values of the chemical potential [66]. This result seems to confirm our expectation that the global properties of the momentum distribution are strongly dominated by the behavior of the system at the trap center, which best approximates the bulk behavior.

To make this connection even more quantitative, we can consider again the partition of the system into a central  $C$  region and a complementary peripheral  $\bar{C}$  region as a partition of the trapped gas into a system

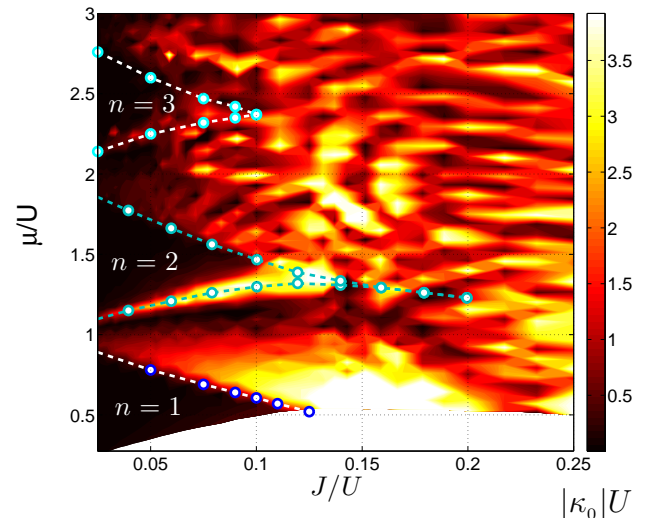


FIG. 20: Absolute value of the condensate compressibility  $\kappa_0 = \partial n(k=0)/\partial \mu$  (in units of  $U^{-1}$ ) of  $N = 100$  bosons under variable trapping frequency.

and a particle reservoir, respectively (Fig. 1). Trap squeezing increases the chemical potential of the reservoir with respect to that of the system, and it hence pumps particles from the former to the latter. If the system experiences (quasi-)condensation, a (quasi-)macroscopic fraction of the pumped particles will enter the (quasi-)condensate. Alternatively, if the central region has a density which approaches an integer value from below,  $n_C < \text{int}(n_C) + 1/2$ , condensation should be rather

thought of in terms of holes (of density  $\text{int}(n_C) + 1 - n_C$ ); in that case a (quasi-)macroscopic fraction of the holes removed from the center under trap squeezing belongs to the (quasi-)condensate. In both cases, if the trap center is in a local (quasi-)condensate state, one expects that the variations of the  $n(k=0)$  peak in the momentum distribution will be proportional to (for true condensation) or will go as a power law of (for quasi-condensation) the variation of the density in the trap center. On the other hand, if the center of the trap is in a MI insulating phase, this prevents the particle (hole) transfer, and it inhibits the variations of the momentum distribution.

From the above arguments, one expects the behavior of the momentum distribution to be extremely sensitive to trap squeezing; this sensitivity can be quantified by the *condensate compressibility*

$$\kappa_0 =: \frac{\partial}{\partial \mu} n(k=0) \quad (33)$$

which can capture the (quasi-)macroscopic transfer of particles from the  $\bar{C}$  reservoir into a condensed state in the center  $C$  (or viceversa for hole condensation). The condensate compressibility is positive for particle (quasi-)condensation in the trap center, and negative for hole (quasi-)condensation. Consequently  $|\kappa_0|$  is expected to be finite in presence of condensation in  $C$  (apart from the zeros corresponding to the passage from particle to hole condensation), and to be essentially vanishing corresponding to MI behavior. Fig. 20 confirms this expectations, showing that  $|\kappa_0|$  is vanishing corresponding to the bulk MI regions (apart from the usual blue shift of the critical chemical potentials) while it has generally finite values corresponding to the SF regions. The behavior in the SF regions is highly inhomogeneous, due to the frequent passage from particle to hole condensation. In any case, one can easily tell apart the accidental vanishing of the condensate compressibility in a SF regime from the systematic vanishing in the MI regime *e.g.* by inspection of the FWHM, which is much smaller than  $2\pi/a$  in the SF case, and of the order of  $2\pi/a$  in the MI case ( $a$  being the lattice spacing).

## VII. APPLICATIONS: BOSE GLASS IN A THREE-COLOR SUPERLATTICE

### A. Signatures of a Bose glass

In the previous section we have seen that trap squeezing allows to faithfully reconstruct the phase diagram of the ordinary Bose-Hubbard model, either via the measurement of the diagonal properties in the central region of the trap, or via the measurement of the evolution of the global off-diagonal properties (momentum distribution). This latter aspect is due to the fact that spectral properties and coherence properties can both characterize fully the two phases (SF and MI) present in the phase diagram of the Bose-Hubbard model. On the other hand, spectral

and coherence properties become complementary pieces of information in presence of disorder in the system, inducing a novel phase in the phase diagram: the Bose glass [8]. This extra phase is in fact characterized by a finite compressibility coexisting with short-range phase coherence, and it needs the joint measurement of local diagonal properties and global momentum distribution to be detected.

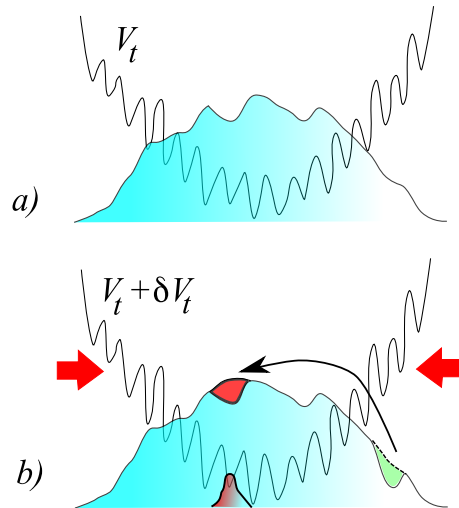


FIG. 21: Trap squeezing in the Bose glass phase. *a)* Schematic view of the density profile of a boson gas in a disordered optical lattice. *b)* In presence of a Bose glass behavior in the trap center, upon infinitesimal trap squeezing  $V_t \rightarrow V_t + \delta V_t$  a particle can be transferred from the trap wings to a *localized* state in the center. Due to its localized nature, this additional particle does not contribute significantly to the coherent fraction, which remains essentially unchanged.

In Ref. [30] we have shown that trap squeezing can reveal the Bose glass phase appearing in the Bose-Hubbard model with a one-color quasi-periodic potential, realized by a two-color incommensurate optical superlattice [22, 36, 67, 68]. The fingerprint of the Bose glass in a trap is the observation of a finite central compressibility  $\kappa_C$ , coexisting with a weak condensate compressibility  $\kappa_0$ , and with the observation of a broad peak in the momentum distribution.

Fig. 21 sketches the response to trap squeezing of a Bose glass occurring in the trap center. By definition, the Bose glass phase admits particle excitations at arbitrarily low energy, which means that a small increase in the trap frequency  $V_t$  and, consequently, in the global chemical potential  $\mu$ , is able to transfer a particle to the center of the trap, resulting in a finite central compressibility  $\kappa_C$ . It is important to emphasize that this is only true *on average over the disorder distribution*: indeed, averaging over the disorder statistics, one expects always the existence of one or several disorder arrangements in the trap center which admit the transfer of a particle from the wings to the center at an infinitesimal energy cost. Explicit disorder averaging is crucial, because we

cannot expect in general the central region of the system to be self-averaging, due to its relatively small size. In the following we will consider quasi-periodic superlattices, which admit random relative spatial phases between the various Fourier components. In this case, the full disorder statistics in the trap is sampled by considering different values of the relative phases.

If the shift in chemical potential associated with trap squeezing is not bringing the system across a Bose-glass-to-superfluid transition, the particles that are transferred from the wings to the center will occupy *localized* quasi-particle states - meaning that the density variation that their transfer causes will be well localized in space. This implies that the new particle appearing in the center remains highly spread in momentum, and that it only contributes a small amount to the  $k = 0$  peak in the momentum distribution. As a consequence, the coherence properties are only weakly altered by the particle transfer, and the condensate compressibility remains small.

While a finite central compressibility  $\kappa_C$  is a solid criterion (and a pre-requisite) for the identification of a Bose glass, it is *a priori* more difficult to fix a criterion on the condensate compressibility which would distinguish a Bose glass from a weakly correlated superfluid. In fact, in both cases the condensate compressibility is generally finite, given that a global increase of the density leads to a global change of the momentum distribution, regardless of whether the system exhibits condensation or not. The only rigorous approach to discriminate a compressible insulator from a condensate is to study the scaling of the condensate occupation  $n(k=0)$  under increasing particle number and decreasing trapping frequency, namely at *fixed chemical potential*; this will be the subject of a future publication. Nonetheless, a semi-quantitative criterion can be formulated based on the width of the momentum distribution. Indeed the inverse of the FWHM of such a peak gives an estimate of the correlation length  $\xi$  in the system: in the following we will take  $\xi \approx 2(\text{FWHM})^{-1}$  (based on the assumption that the momentum distribution  $n(k)$  can be approximated by a Lorentzian with parameter  $\xi$ ). The system is obviously in an insulating state if  $\xi$  is far below the width of the atomic cloud. We can estimate such a width via the *participation ratio*

$$\text{PR} = \frac{N^2}{\sum_i \langle n_i \rangle^2} . \quad (34)$$

Hence the system can be safely considered as an insulator if  $\xi \ll \text{PR}$ .

### B. Three-color incommensurate superlattice

We now focus our attention on the  $1d$  Bose-Hubbard in a two-color quasi-periodic potential, Eq. (17), realized via a three-color incommensurate superlattice. In Ref. [36] we have shown that this potential, despite being quasi-random, appears to support a Bose-glass phase

over a continuous region of the phase diagram. This is to be contrasted with the one-color quasi-periodic potential, realized via two-color superlattices [22], which features Bose glass behavior as well as incompressible incommensurate-band-insulator behavior [36, 67], appearing in a tight alternation upon varying the chemical potential. In other words, while the one-color potential still retains features of its quasi-periodic nature, the two-color potential seems to mimic very closely the behavior of a purely random potential.

In the following we focus indeed on the regime in which the system immersed in a two-color potential exhibits an extended Bose-glass phase, namely for potential strength  $V_2 = U$  which removes completely the Mott insulator from the phase diagram. In particular we consider the case of a strong potential,  $V_2 = 20J$ , which establishes a Bose glass for all the values of the chemical potential we have explored. The trapped version of the system is investigated in the case of  $N = 100$  bosons, and under averaging over the spatial phases  $\phi, \phi'$  of the Fourier components of the potential, Eq. (17). In particular we investigate the behavior of the phase-averaged quantities: the central density  $\langle n_C \rangle_\phi$ , the momentum distribution  $\langle n(k) \rangle_\phi$  and its FWHM, and the participation ratio  $\langle \text{PR} \rangle_\phi$ . We will plot these quantities as a function of the phase-averaged chemical potential, which in Section III has been shown to satisfy a simple scaling relationship as a function of the experimental parameters  $V_t$  and  $N$ . The data on the trapped system are compared with those of the bulk system, realized by a chain of  $L = 300$  sites for a fixed value of the potential phases  $\phi, \phi'$ ; in this case disorder averaging is provided by the extended size of the system, which shows to be fully self-averaging (we have explicitly checked this aspect by comparison with an even longer chain,  $L = 500$ ).

Fig. 22 shows the evolution of the central density in the trapped system for a central region  $C$  of varying size, compared with the bulk behavior. The bulk behavior shows a continuous variation of the density with the chemical potential, signaling a finite compressibility over the whole range we have considered. We observe that the phase-averaged central density closely follows the bulk behavior, and, in the case of  $N = 100$  bosons we consider, the dependence of the central density on the size of the  $C$  region is very weak up to densities  $n \lesssim 2$ , signaling that a faithful measurement of the  $n(\mu)$  curve can be achieved at different imaging resolutions. To faithfully reproduce the behavior at higher densities it is necessary to have a good resolution of around 10 sites, or, alternatively, to increase the number  $N$  of trapped particles and reduce the trapping potential (thereby keeping the product  $N^{2/3}V_t^{1/3}$  constant) in order to increase the quasi-homogeneous region in the trap center.

The insulating nature of the phase stabilized in the trap center is revealed by the momentum distribution. In Fig. 23 we show the evolution of the peak in the momentum distribution under trap squeezing. The comparison with the data of the bulk system shows that the

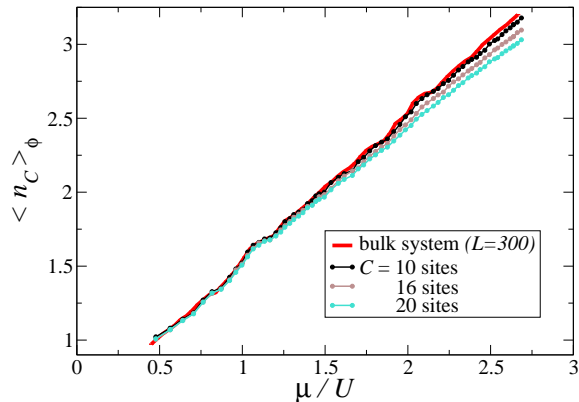


FIG. 22: Phase-averaged central density of a system of  $N = 100$  one-dimensional bosons trapped in a parabolic potential plus a three-color superlattice, Eq. (17) (see text for the parameters). The results for the trapped system are compared with those of a bulk system with  $L = 300$  sites.

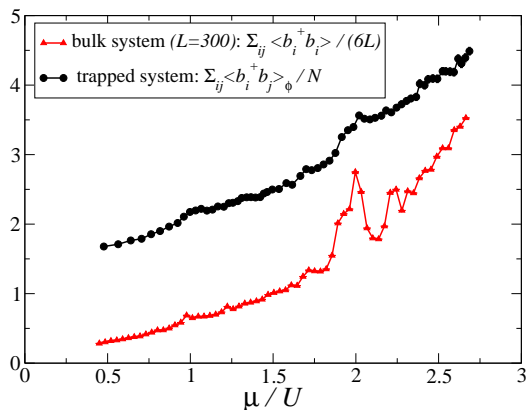


FIG. 23:  $k = 0$  peak in the momentum distribution for a system of  $N = 100$  one-dimensional bosons trapped in a parabolic potential plus a three-color superlattice (same as in Fig. 22). The results are compared with those of a bulk system with  $L = 300$  sites.

trapped system reproduces the main features of the bulk behavior, including some subtle ones (for instance, the anomaly for  $\mu/U \approx 2$ ); this further confirms that the momentum distribution is dominated by the behavior in the trap center, which best approximates the bulk behavior. In the case of the bulk system, the inspection of the superfluid density [36] allows to conclude that the system is in an insulating state for all explored chemical potentials, as the superfluid density turns out to be identically vanishing everywhere. This conclusion cannot be

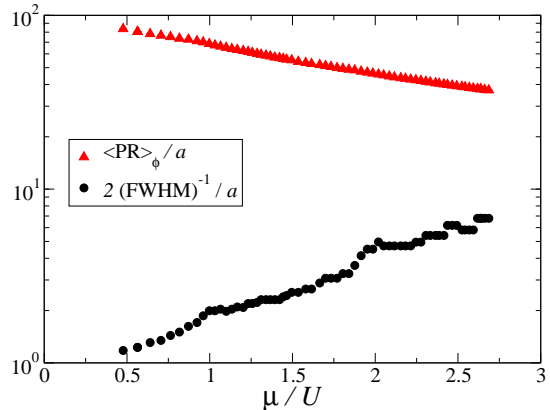


FIG. 24: Correlation length of system of  $N = 100$  one-dimensional bosons trapped in a parabolic potential plus a three-color superlattice (same as in Fig. 22), estimated via the inverse FWHM of the momentum distribution. This quantity is compared with the effective cloud size, given by the phase-averaged participation ratio.

easily drawn on the basis of the observation of the momentum distribution. In fact, at variance with the Mott insulating state, the condensate compressibility  $\kappa_0$  appears to be finite everywhere, although large excursions of the chemical potential (*e.g.* from  $0.5 U$  to  $U$ ) only slightly change the condensate population (by about 10% in the case mentioned). As already mentioned, the most dramatic signature of the insulating behavior would be revealed upon scaling the system size. Yet, in this case the insulating behavior is so pronounced that it is already revealed at the level of the single system size we considered. In fact, as shown in Fig. 24, the correlation length estimated via the inverse of the full width at half maximum is considerably smaller than the system size, estimated via the participation ratio (it is more than an order of magnitude smaller for  $\mu/U \lesssim 2$ ). Hence the observation of the central density and its evolution under trap squeezing, together with the measurement of the momentum distribution, would experimentally allow to conclude unambiguously about the Bose-glass nature of the phase realized in this system.

## VIII. CENTRAL VS. GLOBAL COMPRESSIBILITY

Recent experiments have probed for the first time the compressibility of a fermionic gas in an optical lattice via trap squeezing and *in situ* imaging of the cloud width [31]. The same technique is obviously applicable to bosons as well, and it has been proposed as a practical tool for the detection of the Bose glass [69]. Probing the response of the global width of the atomic cloud to

trap squeezing has the obvious advantage that the imaging resolution required in this case is much less than that demanded by the technique we propose. Here we would like to point out a few drawbacks, particularly associated with the detection of the Bose-glass phase. A discussion of the drawbacks for the case of repulsive fermions can be found in Ref. 51.

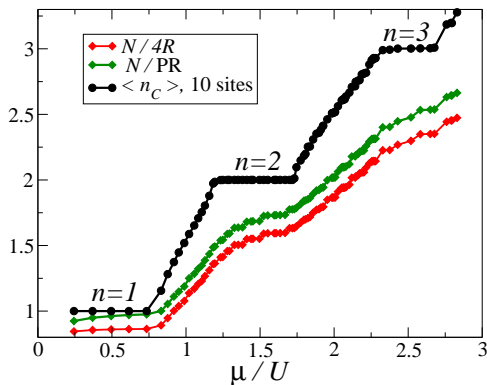


FIG. 25: Central density (averaged over 10 sites) of a system of  $N = 100$  trapped bosons, described by the one-dimensional Bose-Hubbard model with  $U = 20J$  in a parabolic trap. This quantity is compared with the effective global density of the atomic cloud, estimated via the inverse of the cloud radius  $R$  and via the inverse of the participation ratio.

In Ref. 31 the cloud width is estimated via the *cloud radius*, namely the second moment of the density distribution  $\langle n_i \rangle$  [70] (centered around the origin)

$$R = \sqrt{\frac{1}{N} \sum_i |r_i|^2 \langle n_i \rangle}. \quad (35)$$

The response of the atomic cloud to the variation of the trap frequency is then quantified in terms of the variation in the cloud radius  $R$ ; given that  $N/R^d$  gives an estimate of the effective average density of the cloud, one can define a *global cloud compressibility*  $\kappa_g$  as the derivative of  $R^{-d}$  with respect to the trapping potential

$$\kappa_g = -\frac{1}{R^{d+1}} \frac{\partial R}{\partial V_t}. \quad (36)$$

This is a measure of the compressibility of an inhomogeneous trapped system, which collects contributions from all its various parts. In particular, no matter what state the system core is in, the dilute halo around the core is always in a compressible state, so that the global compressibility is necessarily always finite, although it will be significantly higher or smaller depending on whether the core is in a locally compressible state or not. Hence the realization of a specific bulk phase in the system core

does not result in a *qualitatively* different behavior of the global compressibility, but only a *quantitatively* different one. This aspect makes the discrimination of the phases realized in the system core very hard, and even more so the location of the phase boundaries. In particular, as we will discuss below, the identification of some phases might even be completely missed.

Fig. 25 shows the global density  $N/R$  for 100 bosons described by the 1d Bose-Hubbard model with  $U = 20J$  and for a variable trapping potential, controlling the chemical potential of the system. An alternative definition of the global average density, which turns out to be much closer to the true average density, is  $N/PR$ , based on the participation ratio PR, Eq. (34), which gives the effective volume occupied by the system. The PR is very close to size of the region over which the atomic density is non-zero, while the cloud radius  $R$  is closer to the FWHM of the density profile. Despite the apparent variety in the definitions, Fig. 25 shows that  $N/R$  and  $N/PR$  exhibit precisely the same behavior, and they essentially differ by a multiplicative factor. Hence we will use them interchangeably in the following.

In Fig. 25 the global densities  $N/R$  and  $N/PR$  are compared with the central density  $\langle n_c \rangle$  for a central region of 10 sites - as shown in Ref. 30 for the same parameter set, this latter quantity reproduces rather faithfully the density of the bulk system. For the chemical potential excursion considered in this study, we observe three Mott plateaus, which are clearly manifested in the central density, and which also show up in the global densities via a significant change of slope in the dependence on the chemical potential [71]. In this case one could argue that the global compressibility contains essentially the same information as the central one. At the same time, it is evident that important pieces of information are missing in the global compressibility: under the assumption that a loss in global compressibility is always equivalent to the appearance of an incompressible phase in the system core, it is quite hard to locate the phase boundaries between core-compressible and core-incompressible phases, as the changes in slope are quite smooth (despite the commensurate-incommensurate transitions in the core being very sharp for what concerns the central compressibility, as we have already discussed in Sec. VI). Moreover, the global densities contain very little information on the central density at which the core-incompressible phases are realized. As a general remark, one could say that the global density and global compressibility can give information on the alternation of phases and their nature provided that one has a *prior* knowledge of the topology of the phase diagram of the system, and of the particular phases that are realized there.

A much harder (yet more general) situation is the one in which one does not know the succession of phases realized in the system - although the set of the possible phases might still be known. This is a generic situation in which one would like an analog quantum simulator to work. As an example of a complex phase diagram,

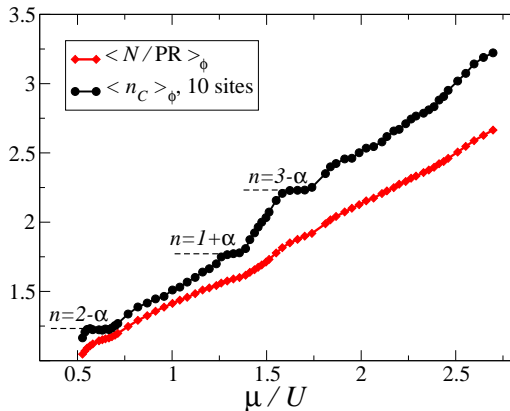


FIG. 26: Central density (averaged over 10 sites) of a system of  $N = 100$  bosons trapped in a parabolic potential plus a two-color incommensurate superlattice (see text). This quantity is averaged over different realizations of the relative spatial phase of the superlattice. Comparison is made with the global density, estimated via the phase-averaged inverse participation ratio.

we consider the case of the Bose-Hubbard model in an incommensurate one-color potential [36, 67, 68]. As already mentioned elsewhere in this paper, this system exhibits four bosonic phases: Mott insulator, superfluid, Bose glass, and incommensurate band insulator. Following Ref. [36], we consider a system of  $N = 100$  bosons in a strong incommensurate potential  $V_2 = U = 20J$  with incommensuration parameter  $\alpha = 830/1076$ , and under variable trapping potential. Fig. 26 shows the phase-averaged global density of such a system  $\langle N/PR \rangle_\phi$ , compared with the phase-averaged central density  $\langle n_C \rangle_\phi$  for a region of 10 sites. As seen in Ref. 36 this latter quantity reproduces most of the features of the density of a bulk system for low enough values,  $n \lesssim 2.5$ . In particular a distinctive feature is represented by plateaus at incommensurate densities, related to the potential parameter  $\alpha$ , and corresponding to incommensurate band insulating phases. The plateau regions are separated by compressible regions manifesting either Bose glass or superfluid behavior (for such strong external potential the Mott insulator is completely washed out, and no plateau appears at integer densities).

When inspecting the global density, one can still observe a weak decrease of its slope as a function of the chemical potential corresponding to the incommensurate plateaus. Nonetheless, without prior knowledge of the bulk phase diagram, it is very hard to understand the nature of this less compressible behavior. First of all, it is a priori unclear whether a local minimum in the compressibility should always be associated with the appearance of a strictly incompressible behavior in the core,

and, even working under this assumption, the estimate of the phase boundaries is somewhat arbitrary. Moreover, it is not possible in principle to decide whether the less compressible phases correspond to ordinary Mott insulators or to some other form of incompressible insulating state, because one lacks definite information on the filling at the trap center. Hence we can conclude that the global density and compressibility do not allow in general to reconstruct the phase diagram of the Bose-Hubbard model in a quasi-periodic potential.

## IX. CONCLUSIONS

In this paper we have shown how the control on the trapping potential for bosons in optical lattices provides a very practical experimental knob on the total chemical potential of the system. Indeed, even in the strongly correlated case of bosons described by the Bose-Hubbard model with or without an external superlattice potential, the global chemical potential at zero-temperature turns out to be related to the trapping potential (and to the other Hamiltonian parameters) via a simple scaling relation. This relation takes the form of a modified Thomas-Fermi scaling relation, corrected by quantum effects, and valid in the case of large enough densities or weak enough interactions, in which lattice commensuration effects are negligible. Corrections beyond this simple expression are quantitatively captured at the level of a simple lattice mean-field theory (Gutzwiller Ansatz), which agrees surprisingly well with quantum Monte Carlo results. The possibility of tuning the chemical potential via the trap gives access to the exploration of the phase diagram of Hamiltonian models in the grand-canonical ensemble, even if cold-atom experiments are generally performed at a fixed number of particles.

If supplemented with an imaging technique able to measure selectively the average density  $n_C$  in a finite region  $C$  around the trap center, the *a priori* knowledge of the global chemical potential  $\mu$  of the system in an optical lattice allows to reconstruct the density-*vs.*- $\mu$  curve of the model implemented in the experiment *without* the trap. In particular this gives access to the bulk compressibility  $\kappa$ , estimated via the central compressibility  $\kappa_C = \partial n_C / \partial \mu$ . We show that central compressibility measurements tell apart very clearly Mott insulator from superfluid phases, and hence they allow to fully reconstruct the phase diagram of the Bose-Hubbard model at zero temperature in the grand-canonical ensemble. The addition of an incommensurate superlattice [22] introduces Bose glass regions in the phase diagram, whose unambiguous detection can be achieved via the joint measurement of the central compressibility and of the global coherence of the system, as well as its response to trap squeezing.

The broader perspective of a truly useful quantum simulation with cold atoms requires to implement computationally more challenging models than lattice bosons -

*e.g.*, to simulate lattice fermions. To do so with minimal “classical input”, one needs a strategy to know in advance all the parameters of the system without the necessity an *ab-initio* classical simulation of the model of interest. While it is still unclear how to gain *a priori* knowledge on the temperature without extensive classical simulations [17, 18], the case study of the Bose-Hubbard model, presented in this work, suggests that mean-field variational Ansatzes might be successful to reconstruct *a priori* the chemical potential of strongly correlated system in their ground state, even when the same variational Ansatzes do not provide an accurate description of the microscopic behavior of the system.

## X. ACKNOWLEDGEMENTS

We thank L. Fallani for suggesting the imaging technique described in Section V, and M. Rigol for stimulating suggestions.

### Appendix A: Jordan-Wigner fermionization and extended fermionization

Hardcore boson operators  $[b_i, b_j^\dagger] = 0$  ( $i \neq j$ ),  $\{b_i, b_i^\dagger\} = 1$  can be mapped onto spinless fermions  $f_i, f_i^\dagger$  via the Jordan-Wigner transformation [43].

$$b_i^\dagger = f_i^\dagger \prod_{k=1}^{i-1} e^{-i\pi f_k^\dagger f_k}, \quad b_i = \prod_{k=1}^{i-1} e^{i\pi f_k^\dagger f_k} f_i, \quad (\text{A1})$$

so that the Hamiltonian of infinitely repulsive bosons in an external potential  $V_i$  becomes that of non-interacting spinless fermions:

$$\mathcal{H} = -J \sum_i \left( f_i f_{i+1}^\dagger + \text{h.c.} \right) + \sum_i V_i f_i^\dagger f_i \quad (\text{A2})$$

for which we assume open boundary conditions.

This approach has been recently extended to the case of strongly repulsive 1d softcore bosons in a trap [55] for  $U/J > (U/J)_{c,n}$ , where  $(U/J)_{c,n}$  is the critical value for the superfluid-to-Mott-insulator transition at the largest *integer* density  $n$  reproduced locally in the trap. Under this assumption, the density profile in the trap takes a characteristic “wedding-cake” structure, namely regions at densities in the interval  $[m-1, m]$  (with integer  $m$ ) are separated from regions with densities in the interval  $[m, m+1]$  by a sizable Mott plateau at integer density  $m$ . If  $U/J$  is sufficiently large, density fluctuations in the plateau can be neglected, which means that density fluctuations in the  $[m-1, m]$  region are essentially decoupled from those in the  $[m, m+1]$  region, and that the lattice sites in each of these regions only experience density fluctuations between the two extremal values of the average density. This fundamental restriction of the local Hilbert space to a set of two-level systems implies

the possibility of fermionizing each layer of the cake individually (extended fermionization); the fermionization has to be supplemented with the information that particles in the  $m$ -th layer have an effectively larger hopping due to bosonic enhancement  $J \rightarrow mJ$ , and that they feel an overall potential energy  $U(m-1)$  per site. The extended-fermionization Hamiltonian reads then

$$\mathcal{H} = \sum_{i,m} -mJ \left( f_{i,m} f_{i+1,m}^\dagger + \text{h.c.} \right) + \sum_{i,m} [U(m-1) + V_i] f_{i,m}^\dagger f_{i,m} \quad (\text{A3})$$

where  $f_{i,m}, f_{i,m}^\dagger$  are the spinless fermions associated with the  $m$ -th layer.

### Appendix B: Thomas-Fermi results for the atom number distribution in low-dimensional systems

We consider a gas of weakly interacting bosons in a three-dimensional trap of frequencies  $(\omega_x, \omega_y, \omega_z)$  and in a standing wave potential along  $3-d$  spatial dimensions, defining an array of  $d$ -dimensional trapping elements (tubes for  $d=1$ , pancakes for  $d=2$ ). In the weakly interacting case, we describe the system within Gross-Pitaevskii (GP) theory in continuum space for  $d$  dimensions, and on a lattice for the remaining  $3-d$  ones. To calculate the density profile of the atoms, we make use of the Thomas-Fermi approximation, which amounts to minimizing the potential-energy part of the GP energy functional.

#### 1. $d=1$ (tubes)

In this case the system is immersed in two standing waves along the  $x$  and  $y$  directions, with wavelength  $\lambda_x$  and  $\lambda_y$  respectively, defining a  $2d$  array of tubes. Being  $\mathbf{d}_x = (d_x, 0)$ ,  $\mathbf{d}_y = (0, d_y)$  the vectors of the  $2d$  array, with  $d_\alpha = \lambda_\alpha/2$  ( $\alpha = x, y$ ), we identify the position of the tubes as  $\mathbf{R}(i_x, i_y) = i_x \mathbf{d}_x + i_y \mathbf{d}_y$ . Imagining that the atoms can only occupy the lowest Wannier states of each tube in the  $x$  and  $y$  directions ( $w_x$  and  $w_y$ , respectively), we can discretize the space in those directions, so that the GP wavefunction can be written as  $\Psi = \Psi(i_x, i_y; z)$ . The potential energy part of the associated GP functional reads:

$$E_{\text{GP}}^{(\text{pot})}[\Psi, \Psi^*] = \sum_{i_x, i_y} \int dz \left[ \frac{\tilde{g}^{(1d)}}{2} |\Psi(i_x, i_y; z)|^4 + \left( \epsilon_x i_x^2 + \epsilon_y i_y^2 + \frac{1}{2} m \omega_z^2 z^2 - \mu^{(1d)} \right) |\Psi(i_x, i_y; z)|^2 \right], \quad (\text{B1})$$

where  $\epsilon_\alpha = m \omega_\alpha^2 d_\alpha^2/2$ , and

$$\tilde{g}^{(1d)} = g \int dx dy |w_x(x)|^4 |w_y(y)|^4 \quad (\text{B2})$$

is the effective coupling constant for particles trapped in the lowest Wannier states in the  $x$  and  $y$  direction, related to the bare coupling constant  $4\pi\hbar^2 a_s/m$  ( $a_s = s$ -wave scattering length). Taking a Gaussian approximation for the Wannier states [72] one obtains

$$\tilde{g}^{(1d)} \approx g \frac{k_x k_y}{2\pi} \left( \frac{V_{0x} V_{0y}}{E_{rx} E_{ry}} \right)^{1/4} \quad (\text{B3})$$

where  $k_\alpha = 2\pi/\lambda_\alpha$ ,  $V_{0\alpha}$  is the lattice depth in the  $\alpha$  direction, and  $E_{r\alpha} = \hbar^2 k_\alpha^2 / (2m)$  the associated recoil energy.

The Thomas-Fermi approximation gives for the number of atoms in each tube the expression

$$N^{(1d)}(i_x, i_y) = \int dz \frac{\mu^{(1d)} - (\epsilon_x i_x^2 + \epsilon_y i_y^2 + \frac{1}{2} m \bar{\omega}^2 z^2)}{\tilde{g}^{(1d)}} \quad (\text{B4})$$

where the chemical potential  $\mu^{(1d)}$  is consistently given by:

$$\mu^{(1d)} = \left[ \frac{15 \tilde{g}^{(1d)} d_x d_y N}{8\pi} \left( \frac{m \bar{\omega}^2}{2} \right)^{3/2} \right]^{2/5} \quad (\text{B5})$$

with  $\bar{\omega} = (\omega_x \omega_y \omega_z)^{1/3}$ . Integrating in Eq. (B4) on the region in which the integrand is positive, one finally obtains the expression [73]:

$$N^{(1d)}(i_x, i_y) = \frac{4\sqrt{2}}{3\tilde{g}^{(1d)} \sqrt{m\omega_z^2}} \left( \mu^{(1d)} - \epsilon_x i_x^2 - \epsilon_y i_y^2 \right)^{3/2}. \quad (\text{B6})$$

## 2. $d = 2$ (pancakes)

In this case the system is immersed in a standing wave along the  $z$  direction with wavelength  $\lambda_z$ , defining a  $1d$

array of pancakes. In analogy with what done in the previous section, we define a discretized GP wavefunction  $\Psi = \Psi(x, y; i_z)$ , whose associated potential energy is described by the GP functional

$$E_{\text{GP}}^{(\text{pot})}[\Psi, \Psi^*] = \sum_{i_z} \int dx dy \left[ \frac{\tilde{g}^{(2d)}}{2} |\Psi(x, y, i_z)|^4 + \left( \frac{1}{2} m \omega_x^2 x^2 + \frac{1}{2} m \omega_y^2 y^2 + \epsilon_z i_z^2 - \mu^{(2d)} \right) |\Psi(x, y; i_z)|^2 \right], \quad (\text{B7})$$

where we have introduced the effective coupling constant

$$\tilde{g}^{(2d)} = g \int dz |w_z(z)|^4 \approx g \frac{k_z}{\sqrt{2\pi}} \left( \frac{V_{0z}}{E_{rz}} \right)^{1/4} \quad (\text{B8})$$

with evident meaning of the symbols.

Integrating the Thomas-Fermi expression for the density within each pancake, we obtain the atom number distribution

$$N^{(2d)}(i_z) = \frac{\pi}{m \tilde{g}^{(1d)} \omega_x \omega_y} \left( \mu^{(2d)} - \epsilon_z i_z^2 \right)^2 \quad (\text{B9})$$

with chemical potential

$$\mu^{(2d)} = \left[ \frac{15 \tilde{g}^{(2d)} d_z N}{8\pi} \left( \frac{m \bar{\omega}^2}{2} \right)^{3/2} \right]^{2/5}. \quad (\text{B10})$$

- 
- [1] I. Bloch, J. Dalibard, and W. Zwerger, *Rev. Mod. Phys.* **80**, 885 (2008).
- [2] M. Lewenstein, A. Sanpera, V. Ahufinger, B. Damski, A. Sen (De), and U. Sen, *Adv. Phys.* **56**, 243 (2007).
- [3] R. P. Feynman, *Int. J. Theor. Phys.* **21**, 467 (1982).
- [4] G. Murthy, D. P. Arovas, and A. Auerbach, *Phys. Rev. B* **55**, 3104 (1997).
- [5] M. Boninsegni, *J. Low Temp. Phys.* **132**, 39 (2003).
- [6] P. Sengupta, L. P. Pryadko, F. Alet, M. Troyer, and G. Schmid, *Phys. Rev. Lett.* **94**, 207202 (2005).
- [7] V. W. Scarola, E. Demler, and S. Das Sarma, *Phys. Rev. A* **73**, 051601 (2006).
- [8] M. P. A. Fisher, P. B. Weichman, G. Grinstein, and D. S. Fisher, *Phys. Rev. B* **40**, 546 (1989).
- [9] R. B. Diener, Q. Zhou, H. Zhai, and T.-L. Ho, *Phys. Rev. Lett.* **98**, 180404 (2007).
- [10] T.-L. Ho and Q. Zhou, *Phys. Rev. Lett.* **99**, 120404 (2007).
- [11] B. Capogrosso-Sansone, E. Kozik, N. Prokofev, and B. Svistunov, *Phys. Rev. A* **75**, 013619 (2007).
- [12] L. Pollet, C. Kollath, K. Van Houcke, and M. Troyer, *New J. Phys.* **10** 065001 (2008).
- [13] D. M. Weld, P. Medley, H. Miyake, D. Hucul, D. E. Pritchard, and W. Ketterle, *Phys. Rev. Lett.* **103**, 245301 (2009).
- [14] D. McCay, M. White, and B. DeMarco, *Phys. Rev. A* **79**, 063605 (2009).
- [15] D. McKay, B. DeMarco, arXiv:0911.4143 (2009).
- [16] Q. Zhou and T.-L. Ho, arXiv:0908.3015.
- [17] S. Trotzky, L. Pollet, F. Gerbier, U. Schnorrberger, I. Bloch, N.V. Prokof'ev, B. Svistunov, and M. Troyer, arXiv:0905.4882 (2009).
- [18] R. Joerdens, L. Tarruell, D. Greif, T. Uehlinger, N. Strohmaier, H. Moritz, T. Esslinger, L. De Leo, C. Kollath, A. Georges, V. Scarola, L. Pollet, E. Burovski, E. Kozik, and M. Troyer, arXiv:0912.3790 (2009).
- [19] Q. Zhou, Y. Kato, N. Kawashima, and N. Trivedi, *Phys. Rev. Lett.* **103**, 085701 (2009).

- [20] T.-L. Ho and Q. Zhou, *Nature Phys.* **6**, 131 (2009).
- [21] T. Stöferle, H. Moritz, C. Schori, M. Köhl, and T. Esslinger, *Phys. Rev. Lett.* **92**, 130403 (2004).
- [22] L. Fallani, J. E. Lye, V. Guarrera, C. Fort, and M. Inguscio, *Phys. Rev. Lett.* **98**, 130404 (2007).
- [23] D. Clément, N. Fabbri, L. Fallani, C. Fort and M. Inguscio, *Phys. Rev. Lett.* **102**, 155301 (2009).
- [24] P. T. Ernst, S. Götzke, J. S. Krauser, K. Pyka, D.-S. Lühmann, D. Pfannkuche, K. Sengstock, *Nature Phys.* **6**, 56 (2009).
- [25] K. D. Nelson, X. Li and D. S. Weiss, *Nature Phys.* **3**, 556 (2007).
- [26] T. Gericke, P. Würtz, D. Reitz, T. Langen, and H. Ott, *Nature Phys.* **4**, 949 (2008).
- [27] N. Gemelke, X. Zhang, C.-L. Hung, and C. Chin, *Nature* **460**, 995 (2009).
- [28] W. S. Bakr, J. I. Gillen, A. Peng, S. Fölling, and M. Greiner, *Nature* **462**, 7269 (2009).
- [29] Immanuel Bloch's group website: <http://www.quantum-munich.de/research/single-site-addressing-in-optical-lattices/>
- [30] T. Roscilde, *New J. Phys.* **11**, 023019 (2009).
- [31] U. Schneider, L. Hackermüller, S. Will, Th. Best, I. Bloch, T. A. Costi, R. W. Helmes, D. Rasch, and A. Rosch, *Science* **322**, 1520 (2008).
- [32] S. Fölling, S. Trotzky, P. Cheinet, M. Feld, R. Saers, A. Widera, T. Müller, and I. Bloch, *Nature* **448**, 1029 (2007).
- [33] M. Anderlini, P.J. Lee, B.L. Brown, J. Sebby-Strabley, W.D. Phillips and J. V. Porto, *et al.*, *Nature* **448**, 452 (2007).
- [34] S. Bergkvist, P. Henelius, and A. Rosengren, *Phys. Rev. A* **70**, 053601 (2004).
- [35] S. Wessel, F. Alet, M. Troyer, and G. G. Batrouni, *Phys. Rev. A* **70**, 053615 (2004).
- [36] T. Roscilde, *Phys. Rev. A* **77**, 063605 (2008).
- [37] Y.R.P. Sortais, H. Marion, C. Tuchendler, A.M. Lance, M. Lamare, P. Fournet, C. Armellin, R. Mercier, G. Messin, A. Browaeys, and P. Grangier, *Phys. Rev. A* **75**, 013406 (2007).
- [38] C. J. Pethick and H. Smith, *Bose-Einstein Condensation in Dilute Gases*, Cambridge, 2002.
- [39] A. W. Sandvik, *Phys. Rev. B* **59**, R14157 (1999); O. F. Syljuåsen, *Phys. Rev. E* **67**, 046701 (2003).
- [40] M. Rizzi, D. Rossini, G. De Chiara, S. Montangero, and R. Fazio, *Phys. Rev. Lett.* **95**, 240404 (2005).
- [41] M. Rigol, A. Muramatsu, G. G. Batrouni, and R. T. Scalettar, *Phys. Rev. Lett.* **91**, 130403 (2003).
- [42] M. Rigol and A. Muramatsu, *Phys. Rev. A* **69**, 053612 (2004); *Opt. Commun.* **243**, 33 (2004).
- [43] E. Lieb, Schultz, and D. Mattis, *Ann. Phys. (NY)* **16**, 406 (1961).
- [44] L. Fallani and C. Fort, private communication.
- [45] B. Capogrosso-Sansone, S. G. Syler, N. Prokof'ev, and B. Svistunov, *Phys. Rev. A* **77**, 015602 (2008).
- [46] B. Capogrosso-Sansone, N. V. Prokof'ev, and B. V. Svistunov, *Phys. Rev. B* **75**, 134302 (2007).
- [47] We notice that the  $\mu$  data for the  $d = 3$  system in a superlattice are much more scattered than for all the other cases, as shown on the right panel of Fig. 7. This is due to strong size effects on the system considered, which are inevitable in  $d = 3$  due to the short linear size of each spatial dimension (we have considered cubes with up to  $L = 18$  sites on each side, but the particles are actually confined on a region with linear extent which is even smaller). In presence of a superlattice potential, a system on such a finite size experiences only a few wells of the potential in each spatial dimension, and hence the nonlinearities due to such potential become relevant and cannot be simply averaged out as in the TF/AL approach.
- [48] G. G. Batrouni, H. R. Krishnamurthy, K. W. Mahmud, V. G. Rousseau, and R. T. Scalettar, *Phys. Rev. A* **78**, 023627 (2008).
- [49] M. Rigol, G. G. Batrouni, V. G. Rousseau, and R. T. Scalettar, *Phys. Rev. A* **79**, 053605 (2009).
- [50] R. Jördens, N. Strohmaier, K. Günter, H. Moritz, and T. Esslinger, *Nature* **455**, 204 (2008).
- [51] V. W. Scarola, L. Pollet, J. Oitmaa, and M. Troyer, *Phys. Rev. Lett.* **102**, 135302 (2009).
- [52] T. Kinoshita, T. Wenger, and D. S. Weiss, *Nature* **440**, 900 (2006).
- [53] M. Greiner, O. Mandel, T. W. Hänsch, and I. Bloch, *Nature* **419**, 51 (2002).
- [54] J. Dziarmaga, *Phys. Rev. Lett.* **95**, 245701 (2005).
- [55] G. Pupillo, A. M. Rey, C. J. Williams, and C. W. Clark, *New J. Phys.* **8**, 161 (2006).
- [56] We estimate gaps as small as  $\sim 10^{-4}J$ , and whose smallness might be limited by the resolution of the grid with which we sample the trapping strength.
- [57] A. Aubry and C. André, *Proc. Isr. Phys. Soc.*, ed. C.G. Kuper 3, Adam Hilger, Bristol, 1979.
- [58] J. B. Sokoloff, *Phys. Rep.* **126**, 189 (1985).
- [59] I. B. Spielman, W. D. Phillips, and J. V. Porto *Phys. Rev. Lett.* **98**, 080404 (2007).
- [60] D. J. Han, M. T. DePue, and D. S. Weiss, *Phys. Rev. A* **63**, 023405 (2001).
- [61] W. Ketterle, K. B. Davis, M. A. Joffe, A. Martin, and D. E. Pritchard, *Phys. Rev. Lett.* **70**, 2253 (1993).
- [62] C.-S. Chuu, F. Schreck, T. P. Meyrath, J. L. Hanssen, G. N. Price, and M. G. Raizen, *Phys. Rev. Lett.* **95**, 260403 (2005).
- [63] Y. Shin, C.H. Schunck, A. Schirotzek, and W. Ketterle, *Nature* **451**, 689 (2008).
- [64] Y.-a. Liao, A. S. C. Rittner, T. Paprotta, W. Li, G. B. Partridge, R. G. Hulet, S. K. Baur, and E. J. Mueller, arXiv:0912.0092.
- [65] The standard definition of the lattice momentum distribution would involve a normalization to the volume  $L^d$  of the quantization box, but in the case of a trapped system the quantization box is arbitrary. As an alternative, here we imagine that the quantization box is fixed to the number of bosons  $N$  - which is a convenient convention, given that this number is kept fixed in our study of a trapped system. In this case the condensate occupation  $n(k=0)$  takes the meaning of the number of particles with momenta in the box  $|k| \leq \pi/(aN)$ , where  $a$  is the lattice spacing.
- [66] Ref. 49 has documented that local density signatures of the onset of the Mott phase in a trap show up at a higher  $U/J$  value than in the bulk for one- and two-dimensional systems, and that this blue shift is much more pronounced for higher trapping potentials  $V_t$ . A similar shift has been experimentally documented in K. Jiménez-García, R. L. Compton, Y.-J. Lin, W. D. Phillips, J. V. Porto, and I. B. Spielman, arXiv:1003.1541, based on time-of-flight measurements of bosons trapped in quasi-two-dimensional optical lattices. We find that these observations are fully consistent with our observations for

- the central compressibility (Fig. 16) and for the time-of-flight observables (Fig. 19) of a one-dimensional system, and that they can be easily explained with the fact that the onset of a Mott insulating phase with a small gap  $\Delta$  is hindered by the trap inhomogeneity: indeed the trapping potential discards the Mott insulating behavior beyond a length scale  $|r_i - r_0|$  from the trap center, such that  $V_i(r_i - r_0)^2 \approx \Delta$ .
- [67] G. Roux, T. Barthel, I. P. McCulloch, C. Kollath, U. Schollwck, and T. Giamarchi, Phys. Rev. A **78**, 023628 (2008).
- [68] X. Deng, R. Citro, A. Minguzzi, and E. Orignac, Phys. Rev. A **78**, 013625 (2008).
- [69] D. Delande and J. Zakrzewski, Phys. Rev. Lett. **102**, 085301 (2009).
- [70] In the case of Ref. 31  $\langle n_i \rangle$  is actually the column-integrated density of a three-dimensional system, but this aspect is actually irrelevant for our discussion).
- [71] We avoid extracting the central and global compressibilities by differentiating the related densities, because of the significant numerical noise associated with the derivative. Nonetheless the changes in slope in Fig. 25 are evident.
- [72] W. Zwerger, Journ. of Optics B: Quantum Semiclass. Opt. **5**, S9 (2003).
- [73] A similar formula appears in B. Paredes, A. Widera, V. Murg, O. Mandel, S. Fölling, I. Cirac, G. V. Shlyapnikov, T. W. Hänsch, and I. Bloch, Nature **429**, 277 (2004). That formula matches with ours for the case  $\omega_x = \omega_y = \omega_z$  if the factor of  $5N/(2\pi N(0,0))$  appearing there is changed into its inverse,  $2\pi N(0,0)/(5N)$ . We believe our formula to be correct, as it satisfies the sum rule  $\sum_{i_x, i_y} N^{(1d)}(i_x, i_y) = N$ , which is not satisfied in turn by the formula of Paredes *et al.*